A Simple Hybrid Technique to Reduce Bias of Copolar Correlation Coefficient Estimates

IGOR R. IVIĆ

Cooperative Institute for Mesoscale Meteorological Studies, University of Oklahoma, and NOAA/OAR/National Severe Storms Laboratory, Norman, Oklahoma

(Manuscript received 3 December 2018, in final form 24 June 2019)

ABSTRACT

Estimates of copolar correlation coefficient $|\rho_{hv}(0)|$ are one of the essential products generated by polarimetric weather radars because they are used to discriminate among different scatterer types. In theory, estimates of $|\rho_{hv}(0)|$ take values between zero and one. But, statistical errors may cause the estimates to take values that are outside this interval, in which case they are deemed unusable. This effect is exacerbated if the noise contamination is significant. In addition, even valid $|\rho_{hv}(0)|$ estimates can introduce excessive errors in echo classification if not sufficiently accurate and precise. Consequently, it is vital to produce the $|\rho_{hv}(0)|$ fields populated with estimates of the acceptable accuracy as well as precision and with a minimal number of invalid estimates. To improve $|\rho_{hv}(0)|$ estimation, a simple hybrid technique which produces estimates by combining the outputs of the two previously proposed estimators and the conventional one is presented herein. The technique generates estimates with reduced bias compared to previously proposed estimators. Bias reduction results in an increased number of valid estimates, which translates into improved $|\rho_{hv}(0)|$ fields.

1. Introduction

The implementation of dual polarization on the network of Weather Surveillance Radar-1988 Dopplers (WSR-88Ds) employs simultaneous transmission and reception of electromagnetic waves at horizontal (H) and vertical (V) polarizations (SHV mode) (Doviak et al. 2000). In this mode, the three spectral moments of reflectivity Z, velocity v, and spectrum width σ_v are measured along with polarimetric radar variables of differential reflectivity Z_{DR}, differential phase ϕ_{DP}, and the copolar correlation coefficient $|\rho_{hv}(0)|$ (Doviak and Zrnić 1993).

This work focuses on the estimation of the copolar correlation coefficient (henceforth referred to as the correlation coefficient) in the presence of additive white Gaussian noise. The correlation coefficient is a measure of coherency between horizontally and vertically polarized radar signals. It is used primarily for classification of radar returns (Caylor and Illingworth 1989; Balakrishnan and Zrnić 1990; Brandes and Ikeda 2004; Giangrande et al. 2008; Andrić et al. 2013; Tang et al. 2014). Due to estimator standard deviation and bias, the estimates of $|\rho_{hv}(0)|$ can take values larger than one. This contrasts with the theoretical values of this product which are assumed to be between zero and one. Consequently, if a $|\rho_{hv}(0)|$ estimate exceeds one it can be set to one or marked as invalid for use in classification algorithms. In general, the frequency of invalid estimates tends to increase with decreasing signal-to-noise ratio (SNR) (Ivić 2014) and/or with increasing clutter returns (Friedrich et al. 2009). The former effect is exacerbated in estimators which use the measurements of noise powers in the H and V channel because the accuracy of the H and V noise powers affects the resultant quality of $|\rho_{hv}(0)|$ estimates. One example is the standard lag-0 estimator [Melnikov and Zrnić 2007, their Eq. (2)], which is used on the WSR-88D network and often referred to as the conventional estimator. In this estimator, an erroneous measurement of noise powers in the H and V channels causes incorrect scaling of the cross correlation in the estimator, which leads to bias increase (Ivić 2014). Also, if H and V noise powers are underestimated, the resultant bias is positive and leads to an overall increase in the number of invalid estimates (Ivić 2014). Furthermore, even if noise powers are known accurately, the lag-0 estimator becomes increasingly positively biased as SNR decreases (Liu et al. 1994,

Corresponding author: Igor Ivić, igor.ivic@noaa.gov

DOI: 10.1175/JTECH-D-18-0226.1

Melnikov and Zrnić 2004, Ivić 2014). Thus, in combination with the fluctuation of estimates (i.e., standard deviation), this bias is another major cause of $|\rho_{hv}(0)|$ estimation errors if the conventional estimator is used.

The use of estimated H and V noise powers can be circumvented with the lag-1 estimator (Melnikov and Zrnić 2007) as it does not utilize the noise powers in the computation of $|\rho_{hv}(0)|$ estimates. This estimator, however, requires sufficient coherency between signals from subsequent transmission (i.e., temporal coherency) to produce reliable estimates (Ivić 2014). If sufficient coherency in sample time exists, and if given accurate knowledge of noise powers for lag-0 computations, it has a performance similar to that of the lag-0 estimator. Otherwise, it performs worse than the lag-0 estimator (Ivić 2014, 2016). For this reason, it is not suitable for use in surveillance scans (with unambiguous velocities of $v_a = \sim 9\,\mathrm{m\,s^{-1}}$). Both the lag-0 and the lag-1 estimators become increasingly biased as SNR decreases (Ivić 2014).

To address the noise measurement accuracy issue, a radial-based noise power estimation technique proposed in Ivić et al. (2013) may be used while the inherent positive bias can be mitigated using the technique proposed in Ivić (2016). The latter technique proposes two different algorithms which are applied in surveillance and Doppler scans (with a larger $v_a \approx 30\,\mathrm{m\,s^{-1}}$). The surveillance scan algorithm uses a complex correction procedure with precomputed lookup tables to achieve bias reduction, while a much simpler algorithm, which does not apply lookup table–based corrections, is proposed for Doppler scans. Herein, a novel estimation procedure for surveillance scans is proposed that rivals in simplicity the Doppler scan algorithm, proposed in Ivić (2016), while retaining most of the performance improvement over the conventional estimator.

The paper is organized as follows. In section 2, the conventional lag-0 estimator is analyzed. Next, the proposed $|\rho_{hv}(0)|$ estimation technique is introduced in section 3 and analyzed using simulations. In section 4, the proposed and conventional estimators are applied to real data and their performances are compared. The main contributions of the paper are summarized in section 5.

2. Analysis of the conventional correlation coefficient estimator

For the SHV mode, the conventional lag-0 estimator used by the WSR-88D signal processor is (Melnikov and Zrnić 2007)

$$|\hat{\rho}_{hv}(0)|_{\mathrm{LAG\text{-}0}} = \sqrt{\frac{|\hat{R}_{hv}(0)|^2}{\hat{S}_h \hat{S}_v}}, \tag{1}$$

where it is required that $\hat{S}_h > 0$ and $\hat{S}_v > 0$. The circumflex (^) in Eq. (1) denotes estimates and variables without the circumflex stand for true values. Parameters $\hat{S}_h$ and $\hat{S}_v$ are the estimates of signal powers in the H and V channels, respectively, while $\hat{R}_{hv}(0)$ is the cross-correlation estimate at lag zero (where measurements of complex voltages, or samples, $V_h(m)$ and $V_v(m)$ in the H and V channels at each range location are used to compute these quantities). The lowercase m denotes the transmission within a dwell (or radial) from which the particular voltage originates (i.e., the sample number in sample time). Subsequent transmissions are separated by the pulse repetition time T_s, where $T_s = 1/\mathrm{PRF}$, where PRF is the pulse repetition frequency. A complex voltage sample in the H or V channel is modeled as

$$V_c(m) = V_c^S(m) + V_c^N(m), \quad \text{where} \quad c = \mathrm{h} \quad \text{or} \quad \mathrm{v}, \tag{2}$$

where $V_c^S(m)$ is the signal contribution and $V_c^N(m)$ is the additive white Gaussian noise. Noise samples in H and V are assumed to be statistically independent. Estimates of S_h and S_v (i.e., $\hat{S}_h$ and $\hat{S}_v$) are computed from M sets of samples as

$$\hat{S}_c = \hat{P}_c - N_c = \frac{1}{M}\sum_{m=0}^{M-1} |d(m)V_c(m)|^2 - N_c, \quad \text{where} \quad c = \mathrm{h} \quad \text{or} \quad \mathrm{v}, \tag{3a}$$

while the cross-correlation estimate is

$$\hat{R}_{hv}(0) = \frac{1}{M}\sum_{m=0}^{M-1} d^2(m) V_h^*(m) V_v(m), \tag{3b}$$

where N_h and N_v are the noise power measurements in the H and V channels, and the asterisk denotes complex conjugate. In Eq. (3a), $\hat{P}_h$ and $\hat{P}_v$ are the estimates of total powers, which are the sums of signal and noise powers in H and V, respectively. Also, $d(m)$ stands for signal processing window coefficients imposed on time series (Harris 1978). In the case of weather radars signal processing windows are typically used in the ground filtering process (Torres and Warde 2014) and to improve the azimuthal resolution (Brown et al. 2002; Torres and Curtis 2007).

In the case of the conventional lag-0 estimator, the biases increase exponentially as the SNR decreases

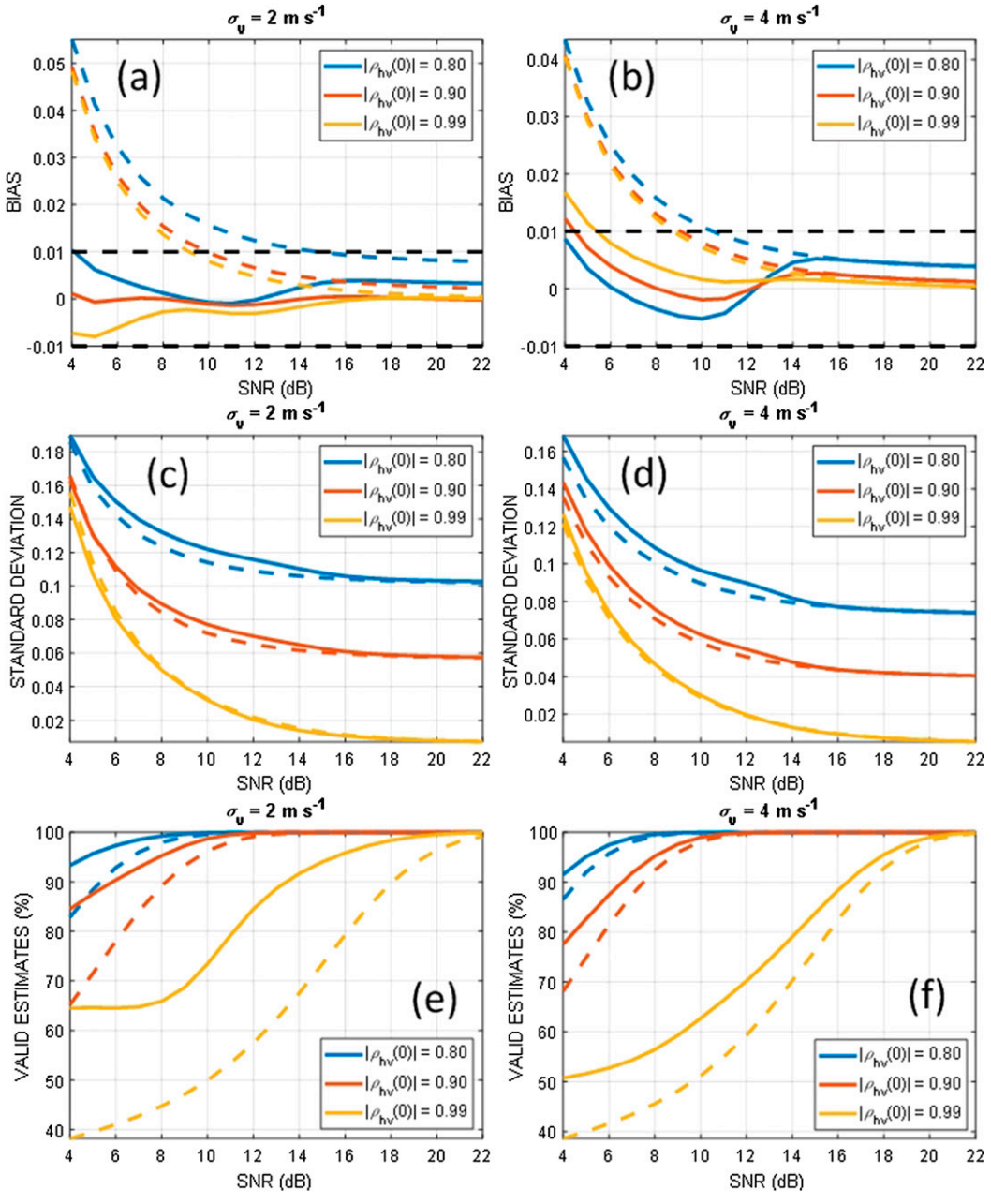

FIG. 1. Results produced by the simple $|\hat{\rho}_{hv}(0)|_{COMB\_S}$ estimator (solid lines) and the lag-0 estimator (dashed lines) for $M = 16$, $v_a = 9\,\mathrm{m\,s^{-1}}$, and $Z_{DR} = 0\,\mathrm{dB}$ showing (a),(b) biases, (c),(d) standard deviations, and (e),(f) valid estimate percentages for $\sigma_v =$ (left) 2 and (right) $4\,\mathrm{m\,s^{-1}}$. Black dashed lines in (a) and (b) represent the desired bias limits.

(Figs. 1a,b). Thus, even if the noise powers are accurately known, the estimates of $|\rho_{hv}(0)|$ are still biased due to the intrinsic sensitivity of Eq. (1) to the SNR. The positive bias, which is evident in Figs. 1a and 1b decreases the number of valid estimates (Figs. 1e and 1f) in the areas of low-to-moderate SNRs (i.e., below 20 dB). Also, classifications of radar returns can be adversely impacted by the positive bias as the lower intrinsic (i.e., true and not measured) $|\rho_{hv}(0)|$ values may be mistaken for higher ones.

The mathematical expectations (denoted by angle brackets) of the numerator and the denominator in the ratio under the square root of the lag-0 estimator are examined to establish the cause of the positive bias. These are given in Ivić (2016) for the case of rectangular window [i.e., $d(m) = 1$] and are generalized here as

$$\langle \hat{S}_h \hat{S}_v \rangle = \frac{1}{M^2} \left\langle \left[\sum_{m=0}^{M-1} |d(m)V_h(m)|^2 - N_h \right] \left[\sum_{n=0}^{M-1} |d(m)V_v(m)|^2 - N_v \right] \right\rangle$$
$$= S_h S_v + \frac{S_h S_v |\rho_{hv}(0)|^2}{M^2} \sum_{m=0}^{M-1} d^4(m)$$
$$+ \frac{2S_h S_v}{M^2} |\rho_{hv}(0)|^2 \sum_{m=1}^{M-1} |\rho(m)|^2 \sum_{l=0}^{M-1-m} d^2(l) d^2(l+m) \quad (4a)$$

and

$$\langle |\hat{R}_{hv}(0)|^2 \rangle = \frac{1}{M^2} \left\langle \left| \sum_{m=0}^{M-1} V_h^*(m) V_v(m) \right|^2 \right\rangle$$
$$= S_h S_v |\rho_{hv}(0)|^2 + \frac{P_h P_v}{M^2} \sum_{m=0}^{M-1} d^4(m)$$
$$+ \frac{2S_h S_v}{M^2} \sum_{m=1}^{M-1} |\rho(m)|^2 \sum_{l=0}^{M-1-m} d^2(l) d^2(l+m)$$
$$= S_h S_v |\rho_{hv}(0)|^2 + S_h S_v \frac{(1 + \mathrm{SNR}_h^{-1})(1 + \mathrm{SNR}_v^{-1})}{M^2} \sum_{m=0}^{M-1} d^4(m)$$
$$+ \frac{2S_h S_v}{M^2} \sum_{m=1}^{M-1} |\rho(m)|^2 \sum_{l=0}^{M-1-m} d^2(l) d^2(l+m), \quad (4b)$$

where $|\rho(m)|$ is the magnitude of the autocorrelation coefficient. Given the Gaussian distributed samples $V_h(m)$ and $V_v(m)$, it is [Doviak and Zrnić 1993, their Eq. (6.5)]

$$|\rho(m)| = \exp\left[-\frac{(\pi \sigma_v m / \upsilon_a)^2}{2} \right]. \quad (5)$$

In Eq. (4b), P_h and P_v are the total powers which are the sums of signal and noise powers in H and V, respectively. Also, SNR_h and SNR_v are the SNRs in the H and V channels, respectively. The first terms, in expressions (4a) and (4b), are the desired values of ensemble averages and the rest of the terms contribute to the bias of the estimator. The bias terms are inversely proportional to M which shows that the ensemble averages of the numerator and denominator in the lag-0 estimator are biased for finite M. Further, the bias of $\langle |\hat{R}_{hv}(0)|^2 \rangle$ in Eq. (4b) depends on the SNRs in H and V as well as the spectrum width [through $|\rho(m)|$]. The bias of $\langle \hat{S}_h \hat{S}_v \rangle$ in Eq. (4a) depends only on the spectrum width. Because $\langle |\hat{R}_{hv}(0)|^2 \rangle$ depends on the SNR_h and SNR_v, the bias of $|\hat{\rho}_{hv}(0)|_{\mathrm{LAG\text{-}0}}$ is affected even if the noise powers in H and V are accurately known. Moreover, the second term in Eq. (4b) increases as SNR_h and SNR_v decrease resulting in the increasingly positive bias of $|\hat{\rho}_{hv}(0)|_{\mathrm{LAG\text{-}0}}$ (as can be observed in Figs. 1a,b). The same effect is corroborated by the bias expression of Eq. (A16) in Melnikov and Zrnić (2007).

3. Improved correlation coefficient estimation

In this section, the approach used in Ivić (2016) is applied to devise a simplified estimator that accounts for the dependency of estimates on the SNR in the H and V channels. First, note that the expression (4a) can be written as

$$\langle \hat{P}_h \hat{P}_v \rangle = \frac{1}{M^2} \left\langle \sum_{m=0}^{M-1} |d(m)V_h(m)|^2 \sum_{n=0}^{M-1} |d(m)V_v(m)|^2 \right\rangle$$
$$= P_h P_v + \frac{S_h S_v |\rho_{hv}(0)|^2}{M^2} \sum_{m=0}^{M-1} d^4(m)$$
$$+ \frac{2S_h S_v}{M^2} |\rho_{hv}(0)|^2 \sum_{m=1}^{M-1} |\rho(m)|^2 \sum_{l=0}^{M-1-m} d^2(l) d^2(l+m). \quad (6)$$

Then, the simplification of expressions (6) and (4b) is introduced whereby the influence of spectrum width on the estimates is neglected (i.e., the third term on the right side of both equations is discarded). This yields

$$\langle \hat{P}_h \hat{P}_v \rangle \approx P_h P_v + S_h S_v |\rho_{hv}(0)|^2 \frac{\sum_{m=0}^{M-1} d^4(m)}{M^2} \tag{7a}$$

and

$$\langle |\hat{R}_{hv}(0)|^2 \rangle \approx S_h S_v |\rho_{hv}(0)|^2 + P_h P_v \frac{\sum_{m=0}^{M-1} d^4(m)}{M^2}, \tag{7b}$$

where $|R_{hv}(0)|^2 = S_h S_v |\rho_{hv}(0)|^2$. The dependencies of $\langle \hat{P}_h \hat{P}_v \rangle$ on $|R_{hv}(0)|^2$ and $\langle |\hat{R}_{hv}(0)|^2 \rangle$ on $P_h P_v$ are preserved, and the noise dependency (i.e., dependency on SNR_h and SNR_v) is preserved through $P_h P_v$ as it causes an exponential increase in bias. Expressions (7a) and (7b) demonstrate that the ensemble averages $\langle \hat{P}_h \hat{P}_v \rangle$ and $\langle |\hat{R}_{hv}(0)|^2 \rangle$ are approximately a system of linear equations with unknowns

$$P_h P_v = S_h S_v + S_h N_v + S_v N_h + N_h N_v, \tag{8a}$$

$$S_h S_v |\rho_{hv}(0)|^2. \tag{8b}$$

The system of equations in (7a) and (7b) can be solved to create new estimates as in Ivić (2016)

$$\hat{E}_1 = \frac{M^2}{M^2 - 1} \left[\hat{P}_h \hat{P}_v - \frac{|\hat{R}_{hv}(0)|^2}{M^2} \sum_{m=0}^{M-1} d^4(m) \right] \tag{9a}$$

$$\hat{E}_2 = \frac{M^2}{M^2 - 1} \left[|\hat{R}_{hv}(0)|^2 - \frac{\hat{P}_h \hat{P}_v}{M^2} \sum_{m=0}^{M-1} d^4(m) \right], \tag{9b}$$

where

$$\langle \hat{E}_1 \rangle \approx P_h P_v \quad \text{and} \quad \langle \hat{E}_2 \rangle \approx S_h S_v |\rho_{hv}(0)|^2. \tag{10}$$

Then, an estimate of $|\rho_{hv}(0)|$ can be obtained as

$$|\hat{\rho}_{hv}(0)|_{LE\_1} = \sqrt{\left| \frac{\hat{E}_2}{\hat{E}_1 - \hat{S}_h N_v - \hat{S}_v N_h - N_h N_v} \right|}, \tag{11}$$

where subscript LE denotes that the estimator (11) is based on the linear equations (LEs) above. It is interesting to note that if $M^2/(M^2 - 1)$ is set to one and the second terms on the right sides of Eqs. (9a) and (9b) are discarded, $|\hat{\rho}_{hv}(0)|_{LE\_1}$ becomes equivalent to the conventional estimator. Hence, unlike $|\hat{\rho}_{hv}(0)|_{LAG\text{-}0}$, the estimator in Eq. (11) accounts for the effects of finite sample size M and SNR.

The performance of $|\hat{\rho}_{hv}(0)|_{LE\_1}$ is examined in Fig. 3a in Ivić (2016). It exhibits reduced bias variation as the SNR declines. However, the bias increases as the value of $|\rho(m)|$ decreases. The latter effect is addressed in Ivić (2016) via the correction procedure which substantially adds to the complexity of the estimation process but results in an outstanding bias reduction as shown in Fig. 5 in Ivić (2016).

The second estimator is also built following the approach in Ivić (2016) as

$$|\hat{\rho}_{hv}(0)|_{LE\_2} = \sqrt{\left| \frac{\hat{E}_4}{\hat{E}_3} \right|}, \tag{12}$$

where

$$\hat{E}_3 = \frac{(M-1)^2}{\left[\sum_{m=0}^{M-2} d(m) d(m+1) \right]^2} \left[\mathrm{Re}\{\hat{R}_h(1) \hat{R}_v^*(1)\} - \frac{\hat{E}_2}{(M-1)^2} \sum_{m=0}^{M-2} d^2(m) d^2(m+1) \right] \tag{13a}$$

$$\hat{E}_4 = \frac{(M-1)^2}{\left[\sum_{m=0}^{M-2} d(m) d(m+1) \right]^2} \left[|\hat{R}_{hv}(1)|^2 - \frac{\hat{E}_1}{(M-1)^2} \sum_{m=0}^{M-2} d^2(m) d^2(m+1) \right], \tag{13b}$$

and

$$\hat{R}_c(1) = \frac{1}{M-1} \sum_{m=0}^{M-2} d(m) V_c^*(m) d(m+1) V_c(m+1), \quad \text{where } c = \mathrm{h} \text{ or } \mathrm{v} \tag{14a}$$

$$|\hat{R}_{hv}(1)|^2 = \frac{1}{2(M-1)^2} \left[\left| \sum_{m=0}^{M-1} d(m) V_h^*(m) d(m+1) V_v(m+1) \right|^2 + \left| \sum_{m=0}^{M-1} d(m) V_h^*(m+1) d(m+1) V_v(m) \right|^2 \right]. \tag{14b}$$

Note though that $|\hat{\rho}_{hv}(0)|_{LE\_2}$ herein is denoted as $|\hat{\rho}_{hv}(0)|_{LE\_3}$ in Ivić (2016). In Ivić (2016), $|\hat{\rho}_{hv}(0)|_{LE\_2}$ bias is corrected using a similar procedure as for $|\hat{\rho}_{hv}(0)|_{LE\_1}$, which further contributes to the estimation technique

complexity. The difference with respect to $|\hat{\rho}_{hv}(0)|_{LE\_1}$ is that the performance of $|\hat{\rho}_{hv}(0)|_{LE\_2}$ becomes worse as the spectrum width increases because it uses second-order estimates at lag 1. To simplify the estimation process, $|\hat{\rho}_{hv}(0)|_{LE\_1}$ and $|\hat{\rho}_{hv}(0)|_{LE\_2}$ are used herein without applying the correction procedure. Along with $|\hat{\rho}_{hv}(0)|_{LAG\text{-}0}$, these estimators are combined via the algorithm described in appendix A to produce the combined estimate $|\hat{\rho}_{hv}(0)|_{COMB\_S}$ [referred to as the simple $|\hat{\rho}_{hv}(0)|_{COMB\_S}$ in the further text as opposed to the complex $|\hat{\rho}_{hv}(0)|_{COMB\_S}$ described in Ivić (2016)].

The bias and standard deviation (SD) are used to evaluate the performance of the $|\rho_{hv}(0)|$ estimators. These are computed as

$$\text{BIAS} = \langle |\hat{\rho}_{hv}(0)|_E \rangle - |\rho_{hv}(0)| \tag{15a}$$

$$\text{SD} = \sqrt{\langle |\hat{\rho}_{hv}(0)|_E^2 \rangle - \langle |\hat{\rho}_{hv}(0)|_E \rangle^2}, \tag{15b}$$

where E denotes an estimator used to produce the correlation coefficient estimate (e.g., LAG-0 or COMB_S). An evaluation in terms of bias is based on the recommendation that the bias within ± 0.01 should be sufficient for "*sensing the mixed-phase precipitation and gauging the hail size quantitatively*" (Balakrishnan and Zrnić 1990). It is imperative to keep the bias of the $|\rho_{hv}(0)|$ estimator as small as possible because spatial smoothing of the data is often utilized by algorithms, such as the hydrometeorological classification algorithm (HCA), to reduce the uncertainty of the classification (Lakshmanan 2004). Estimates with minimal fluctuations are also desired to reduce the classification uncertainty. Consequently, SD is a useful metric for estimator comparison to ensure comparable or smaller variability.

Figure 1 shows the BIAS, SDs, and percentages of valid estimates that were obtained for the lag 0 and simple $|\hat{\rho}_{hv}(0)|_{COMB\_S}$ estimators from simulated time series data produced using the techniques described in Zrnić (1975) and Galati and Pavan (1995). The results are presented for rectangular data processing window and typical surveillance-scan collection parameters from the WSR-88D (NOAA 2017). The estimator $|\hat{\rho}_{hv}(0)|_{COMB\_S}$ exhibits smaller biases than the lag-0 estimator (Figs. 1a,b) while maintaining similar standard deviations (Figs. 1c,d) and producing an increased number of valid estimates (Figs. 1e,f).

The comparison of bias performance between the estimation techniques described in Ivić (2016) and herein is given in Fig. 2. The degradation in the simple $|\hat{\rho}_{hv}(0)|_{COMB\_S}$ bias performance is expected because it does not utilize the additional bias correction steps of Ivić (2016). Nonetheless, the simple $|\hat{\rho}_{hv}(0)|_{COMB\_S}$ still produces significant improvement compared to $|\hat{\rho}_{hv}(0)|_{LAG\text{-}0}$ (shown in Fig. 1). A comparison in terms of SD and the percentage of valid estimates is presented in Fig. 3. It indicates almost the same SD performance and a slightly increased percentage of valid estimates for the complex $|\hat{\rho}_{hv}(0)|_{COMB\_S}$ at σ_v of $4\,\text{m s}^{-1}$, but vice versa at σ_v of $1\,\text{m s}^{-1}$.

4. Application to real data

In this section, the simple and complex $|\hat{\rho}_{hv}(0)|_{COMB\_S}$ estimators as well as the $|\hat{\rho}_{hv}(0)|_{LAG\text{-}0}$ estimator are applied to four sets of real time series data from surveillance scans collected by WSR-88Ds. The first dataset (case 1) parameters are $v_a = 8\,\text{m s}^{-1}$ and $M = 16$ while the parameters for the second (case 2) are $v_a = 8.7\,\text{m s}^{-1}$ and $M = 29$, both at elevation of ~0.5°. The third (case 3) and fourth (case 4) dataset are from the same volume scan at elevations of ~0.5° and ~1.5°, respectively, with parameters $v_a = 9\,\text{m s}^{-1}$ and $M = 29$. All four datasets are processed to produce the superresolution data whereby the estimates are computed on a $250\,\text{m} \times 0.5°$ grid (Brown et al. 2002; Torres and Curtis 2007; NOAA 2017). In the WSR-88D superresolution scans, the von Hann window (Harris 1978) is used to compute the spectral moments which yields the effective beamwidth (Zrnić and Doviak 1976) of ~1.08° (as opposed ~1.47° yielded by the rectangular window). Because polarimetric variables are more susceptible to data quality degradation (than spectral moments) caused by the tapered windows, a window less tapered than the von Hann is used to compute these variables (Istok and Ice 2016). This window is dubbed the Meza window and its coefficients are computed as

$$d(m) = 0.75 + 0.25\cos[2\pi(m + 0.5)/M], \tag{16}$$

which results in an effective beamwidth of ~1.23°. The radial-based noise estimator from Ivić et al. (2013) was used to compute the noise power estimates in the H and V channels. To determine the locations contaminated with ground clutter (GC), a weather environment thresholding (WET) was used (Warde and Torres 2015; Warde 2015). Ground clutter filtering was applied to the received voltages at these locations using the CLEAN-AP filter (Torres and Warde 2014) and point clutter removal (NOAA 2017) was employed to minimize the impact of noise power increases, which affected only a few range locations. Because both the complex and simple $|\hat{\rho}_{hv}(0)|_{COMB\_S}$ estimators are designed assuming no presence of ground clutter, they are only used at locations where CLEAN-AP had not been applied; the $|\hat{\rho}_{hv}(0)|_{LAG\text{-}0}$ estimator is used at locations with ground

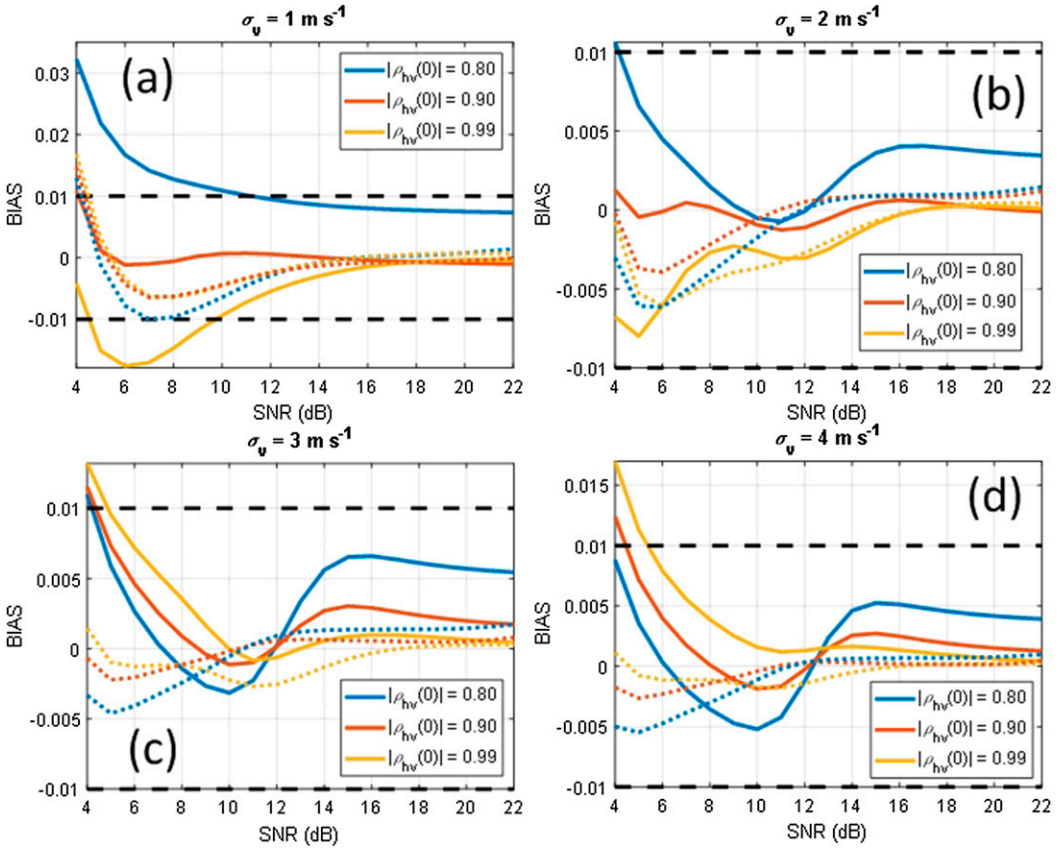

FIG. 2. Bias performances of the simple $|\hat{\rho}_{hv}(0)|_{COMB\_S}$ (solid lines) and complex $|\hat{\rho}_{hv}(0)|_{COMB\_S}$ (dotted lines) estimators for $M = 16$, $v_a = 9\,\text{m s}^{-1}$, and $Z_{DR} = 0\,\text{dB}$ for σ_v = (a) 1, (b) 2, (c) 3, and (d) 4 m s^{-1}. Black dashed lines represent the desired bias limits.

clutter presence. All fields were censored with a 2-dB SNR threshold [standard for WSR-88D reflectivity and $|\rho_{hv}(0)|$ measurements].

The results for the cases 1–4 are shown in Figs. 4–7, respectively. For reference, the SNR_h, reflectivity, and ground clutter classification fields [since $|\hat{\rho}_{hv}(0)|_{COMB\_S}$ is not applied at locations with ground presence] are presented along with results from $|\hat{\rho}_{hv}(0)|_{LAG\text{-}0}$ as well as simple and complex $|\hat{\rho}_{hv}(0)|_{COMB\_S}$ estimators. Colors of light pink and white denote "invalid" points in the fields of correlation coefficient estimates (aka "the pink fringe"). These are generally associated with areas of lower SNR [i.e., areas shown in shades of blue in SNR_h fields in Figs. 4a, 5a, 6a, and 7a] as indicated by simulations. The differences between fields produced using $|\hat{\rho}_{hv}(0)|_{LAG\text{-}0}$ and simple $|\hat{\rho}_{hv}(0)|_{COMB\_S}$ estimators are visible in the areas of lower SNR. Visual inspection of these areas indicates that the simple $|\hat{\rho}_{hv}(0)|_{COMB\_S}$ always produces a larger number of valid estimates than $|\hat{\rho}_{hv}(0)|_{LAG\text{-}0}$. This is supported by Fig. 8 which shows that the simple $|\hat{\rho}_{hv}(0)|_{COMB\_S}$ estimator starts yielding the increasingly higher percentage of valid estimates than $|\hat{\rho}_{hv}(0)|_{LAG\text{-}0}$ as SNR_h drops below ~25 dB. The results in Fig. 8 also show that both simple and complex $|\hat{\rho}_{hv}(0)|_{COMB\_S}$ estimators produce almost the same number of valid estimates for all cases shown. Further indication of equivalent performance may be obtained by visual comparison between the simple and complex $|\hat{\rho}_{hv}(0)|_{COMB\_S}$ fields which do not indicate conspicuous differences. Histograms of $|\hat{\rho}_{hv}(0)|_{LAG\text{-}0}$ as well as simple and complex $|\hat{\rho}_{hv}(0)|_{COMB\_S}$ estimates for locations where $2 < SNR_h < 16\,\text{dB}$ and $SNR_h \geq 16\,\text{dB}$ are given in Fig. 9 (note that the 16-dB threshold was chosen because $|\hat{\rho}_{hv}(0)|_{LAG\text{-}0}$ and simple $|\hat{\rho}_{hv}(0)|_{COMB\_S}$ biases and SDs in Figs. 1a and 1b start to differ at $SNR_h \approx 16\,\text{dB}$). These show that the distributions of estimates from all three estimators are almost the same when $SNR_h \geq 16\,\text{dB}$. If $2 < SNR_h < 16\,\text{dB}$, however, simple and complex $|\hat{\rho}_{hv}(0)|_{COMB\_S}$ histograms are comparable while $|\hat{\rho}_{hv}(0)|_{LAG\text{-}0}$ histogram differs from the other two near $|\hat{\rho}_{hv}(0)| = 1$. This indicates that $|\hat{\rho}_{hv}(0)|_{LAG\text{-}0}$ has higher probability of producing invalid estimates for $|\rho_{hv}(0)|$ values close to one. Consequence is that the histogram means (given in Fig. 9) show that for locations

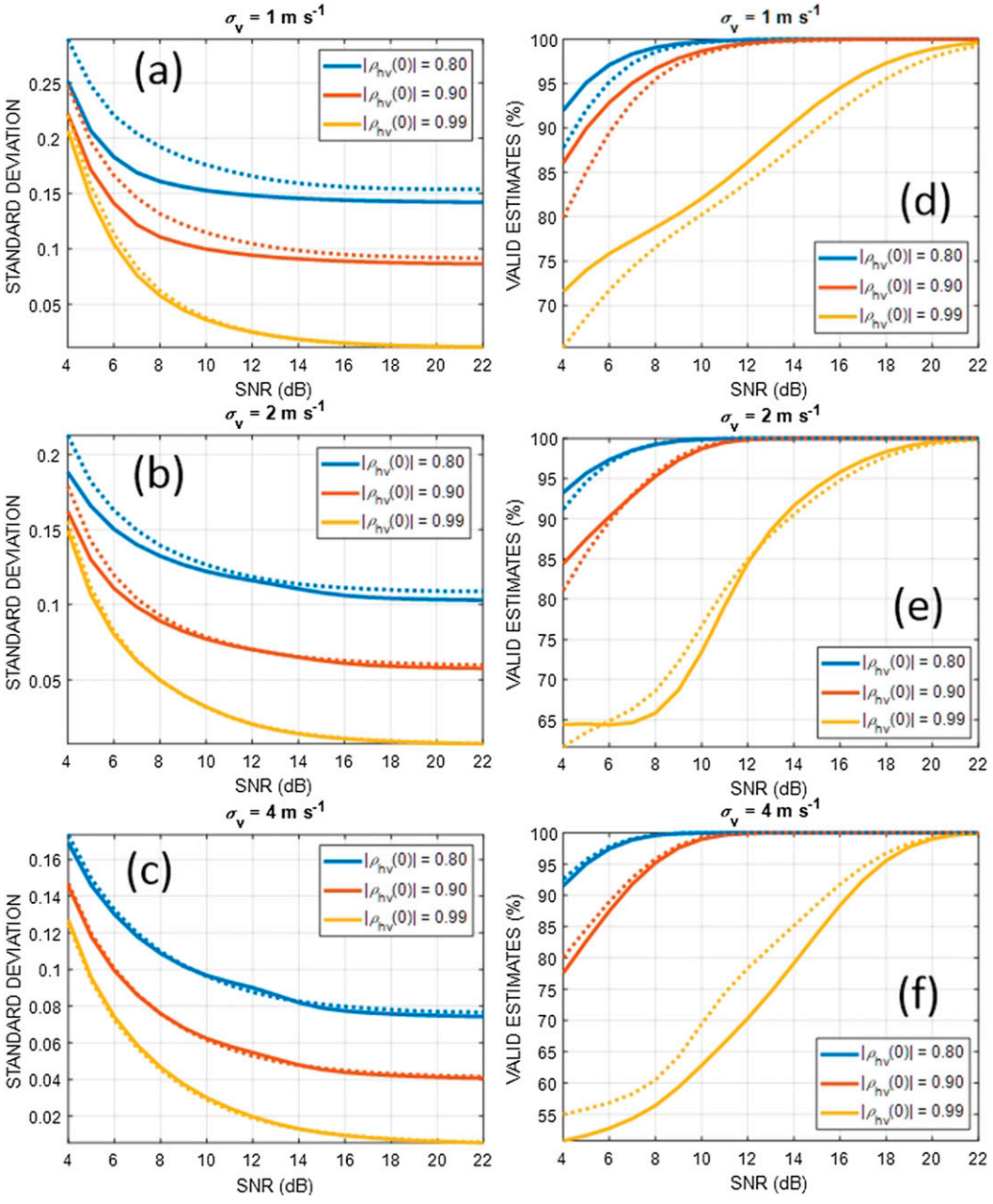

FIG. 3. Bias performances of the simple $|\hat{\rho}_{hv}(0)|_{COMB\_S}$ (solid lines) and the complex $|\hat{\rho}_{hv}(0)|_{COMB\_S}$ (dotted lines) estimators for $M = 16$, $v_a = 9\,m\,s^{-1}$, and $Z_{DR} = 0\,dB$ showing (a)–(c) standard deviations and (d)–(f) valid estimate percentages for σ_v = (top) 1, (middle) 2, and (bottom) $4\,m\,s^{-1}$.

where $2 < SNR_h < 16\,dB$, $|\hat{\rho}_{hv}(0)|_{LAG\text{-}0}$ produces estimates with larger means than the other two estimators. This agrees well with simulation results in Figs. 1a and 1b which show that the conventional estimator becomes increasingly more positively biased than the simple $|\hat{\rho}_{hv}(0)|_{COMB\_S}$ with SNR_h decrease.

The statistics that exemplifies the reduction in the number of invalid estimates as well as the area covered by these estimates is presented in Table 1 while the statistics which demonstrates the increase in the number of valid estimates and the area covered by these estimates is given in appendix B. The last three columns in Table 1 show the percentages of invalid estimates (i.e., invalid points) with respect to the total number of significant returns (i.e., number of points where $SNR_h > 2\,dB$ or total points) for $|\hat{\rho}_{hv}(0)|_{LAG\text{-}0}$, as well as the simple and complex $|\hat{\rho}_{hv}(0)|_{COMB\_S}$. These are computed as

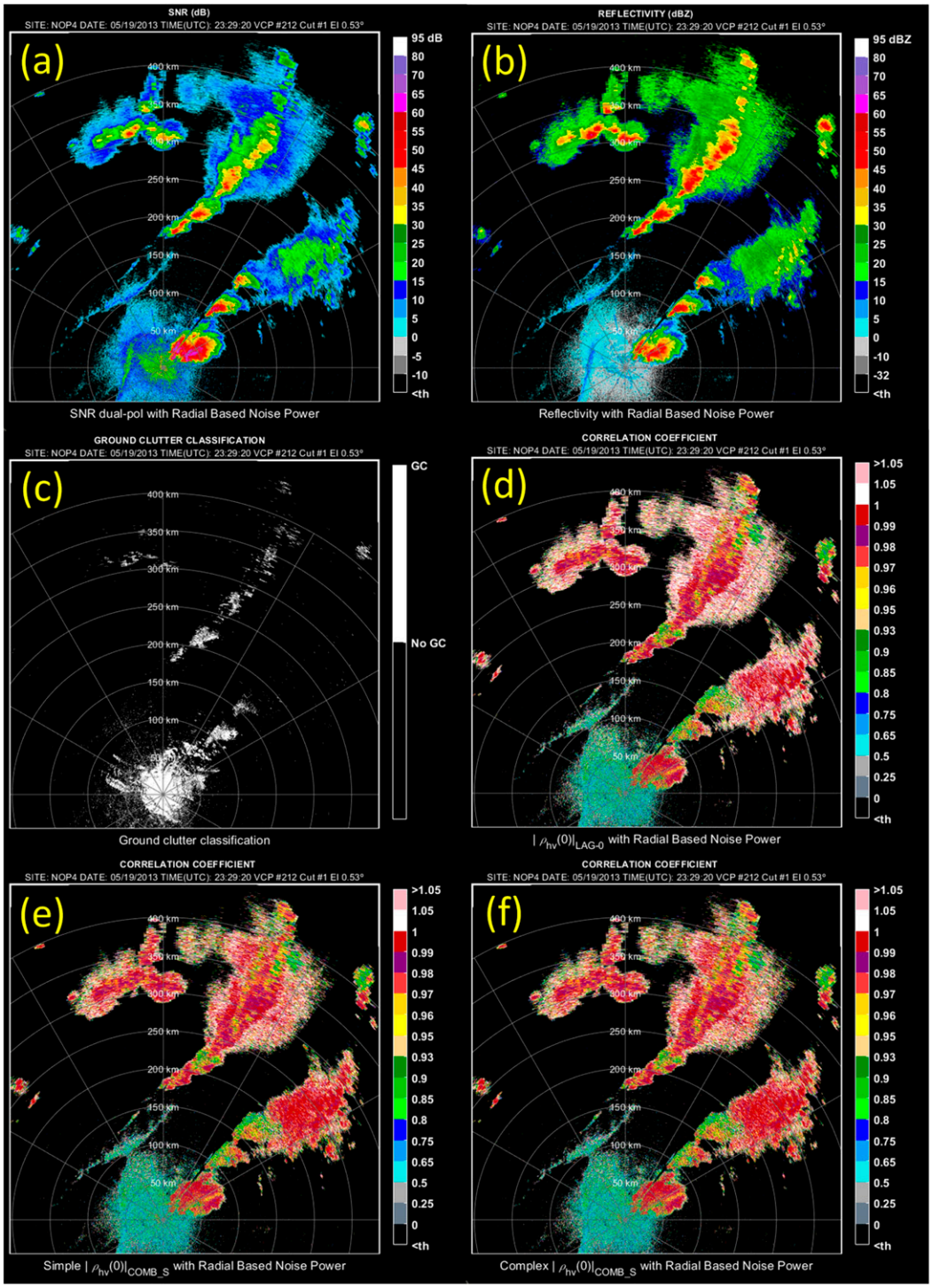

FIG. 4. Case 1 results. (a) SNR and (b) reflectivity fields produced using the radial-based noise estimator. (c) Ground clutter (GC) classification field. Correlation coefficient fields generated using (d) $|\hat{\rho}_{hv}(0)|_{LAG-0}$, (e) simple $|\hat{\rho}_{hv}(0)|_{COMB\_S}$, and (f) complex $|\hat{\rho}_{hv}(0)|_{COMB\_S}$ estimators.

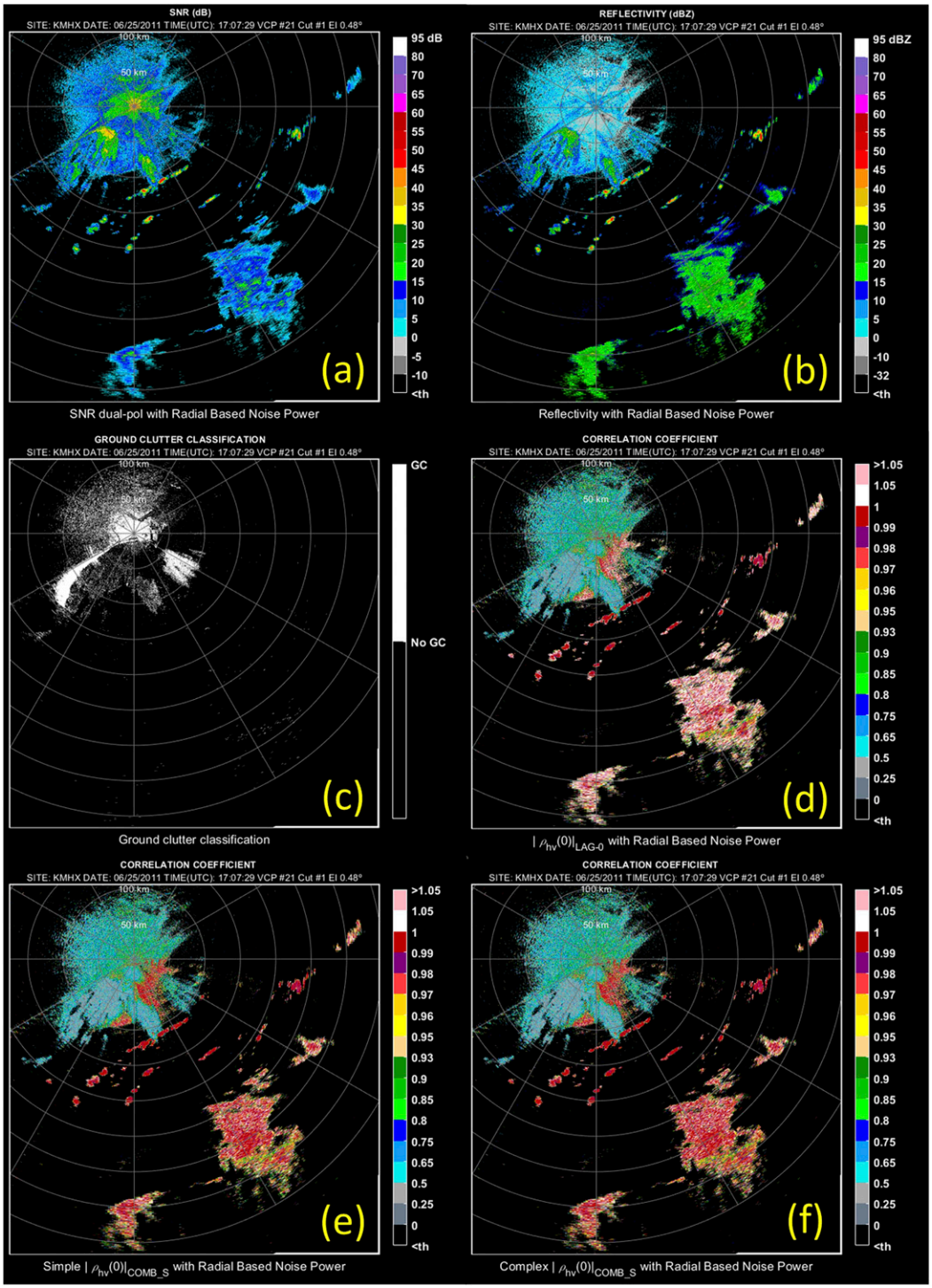

FIG. 5. Case 2 results. (a) SNR and (b) reflectivity fields produced using the radial-based noise estimator. (c) GC classification field. Correlation coefficient fields generated using (d) $|\hat{\rho}_{hv}(0)|_{LAG-0}$, (e) simple $|\hat{\rho}_{hv}(0)|_{COMB\_S}$, and (f) complex $|\hat{\rho}_{hv}(0)|_{COMB\_S}$ estimators.

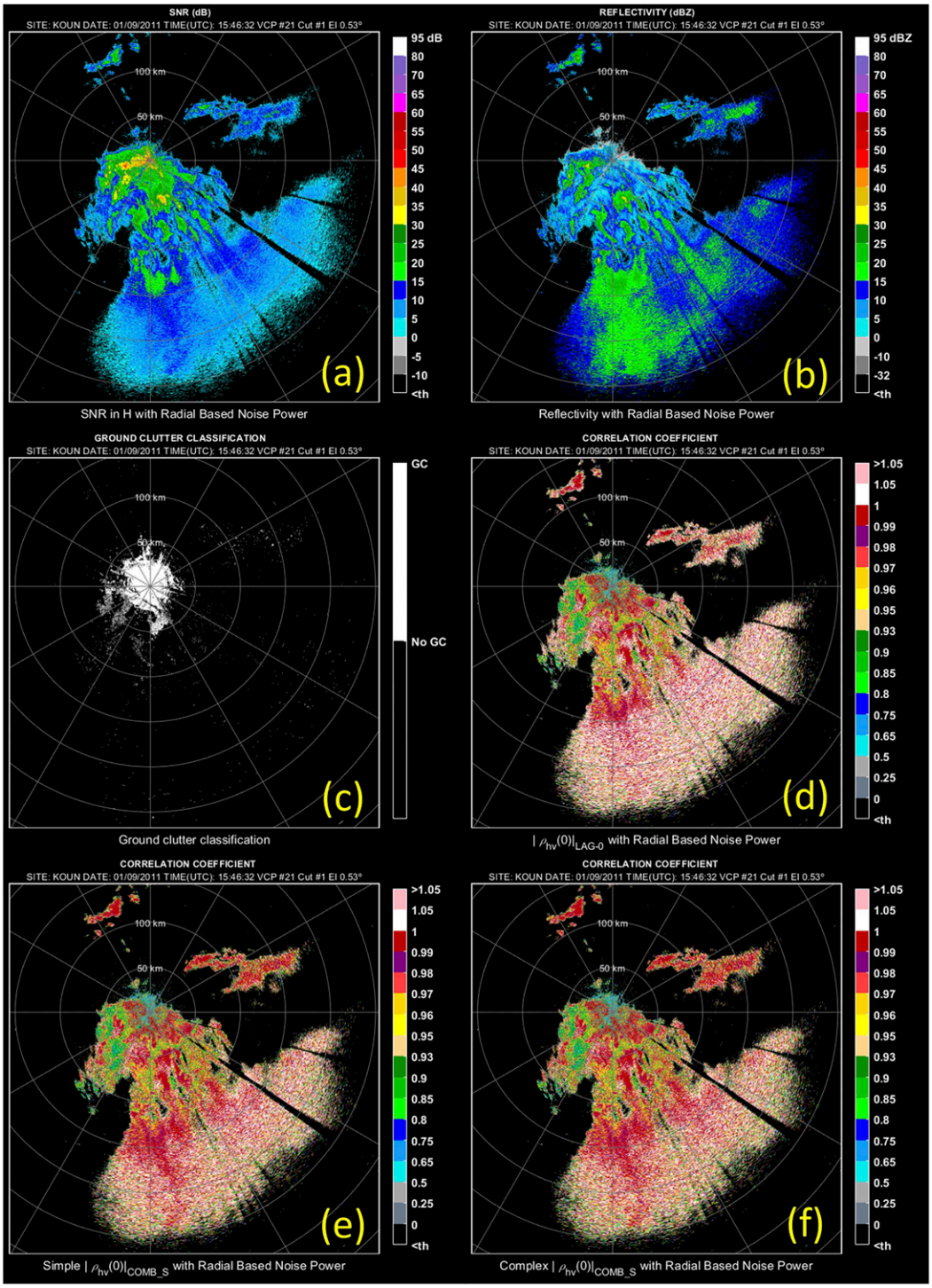

FIG. 6. Case 3 results. (a) SNR and (b) reflectivity fields produced using the radial-based noise estimator. (c) GC classification field. Correlation coefficient fields generated using (d) $|\hat{\rho}_{hv}(0)|_{LAG\text{-}0}$, (e) simple $|\hat{\rho}_{hv}(0)|_{COMB\_S}$, and (f) complex $|\hat{\rho}_{hv}(0)|_{COMB\_S}$ estimators.

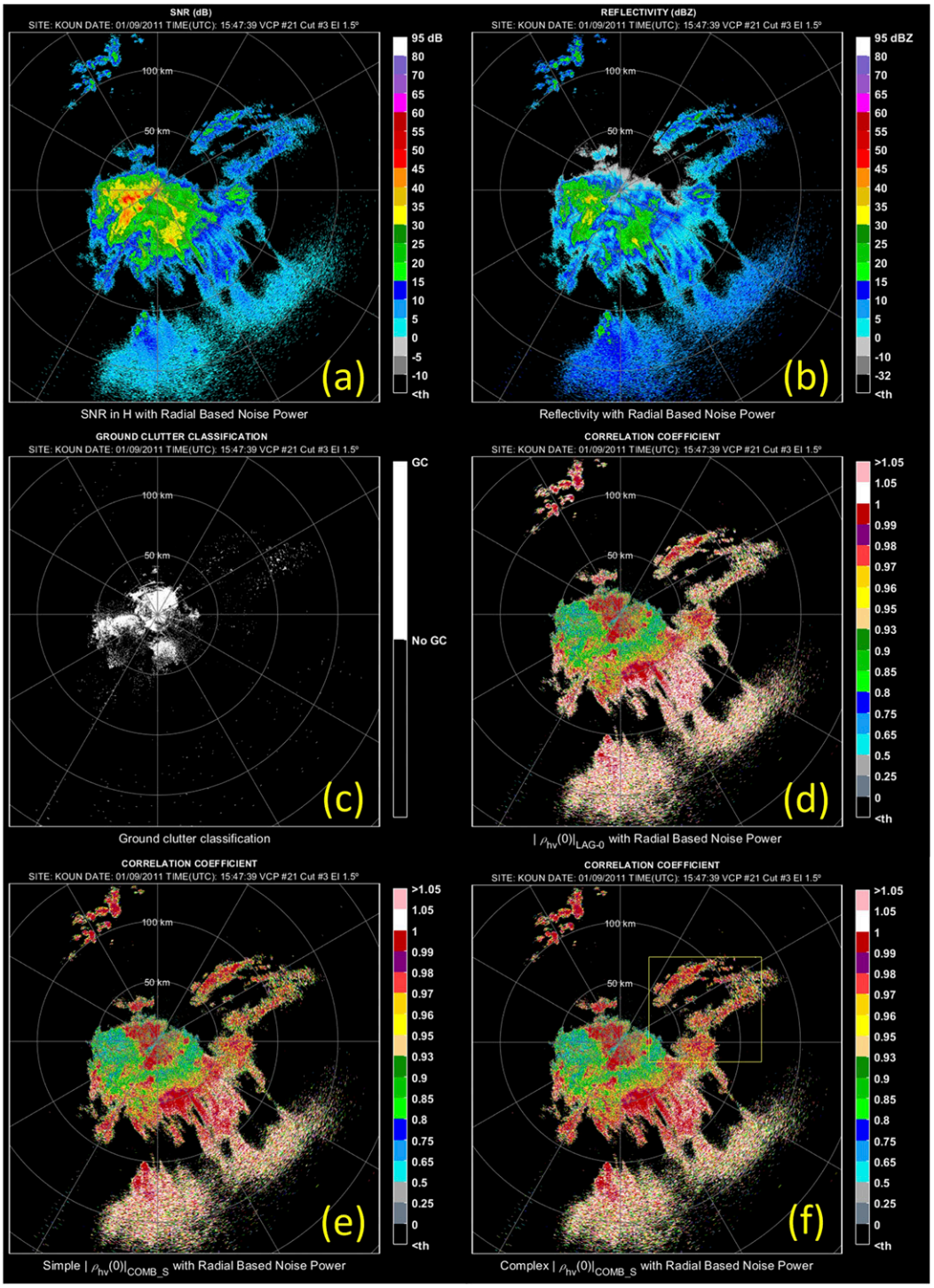

FIG. 7. Case 4 results. (a) SNR and (b) reflectivity fields produced using the radial-based noise estimator. (c) GC classification field. Correlation coefficient fields generated using (d) $|\hat{\rho}_{hv}(0)|_{LAG-0}$, (e) simple $|\hat{\rho}_{hv}(0)|_{COMB\_S}$, and (f) complex $|\hat{\rho}_{hv}(0)|_{COMB\_S}$ estimators.

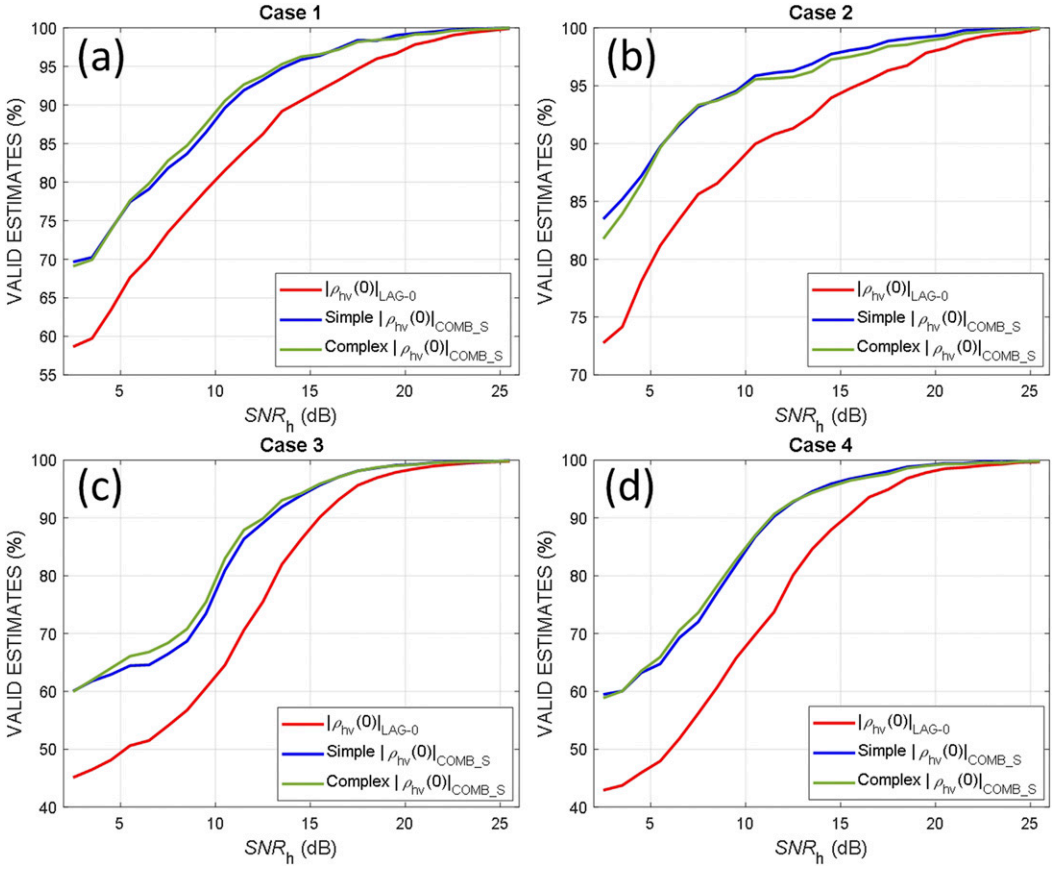

FIG. 8. Percentage of valid estimates as a function of SNR_h for cases (a) 1, (b) 2, (c) 3, and (d) 4.

$$X\text{ invalid points} = \frac{\sum_{n=1}^{\text{Total points}} X^{\text{INV}}(n)}{\text{Total points}} \times 100\%, \quad (17)$$

where X denotes the simple, complex $|\hat{\rho}_{hv}(0)|_{COMB\_S}$ or $|\hat{\rho}_{hv}(0)|_{LAG\text{-}0}$, while $X^{INV}(n)$ is 1 if nth estimate from an estimator X exists (i.e., $SNR_h > 2$ dB) and is invalid while it is 0 otherwise. It also presents the same statistics in terms of area covered by invalid estimates (invalid area) which is computed as

$$X\text{ invalid area} = \frac{\sum_{n=1}^{\text{Total points}} X^{\text{INV}}(n) \times \text{Rng}(n) \times 0.25 \times \frac{\pi}{180} \times 0.5}{\sum_{n=1}^{\text{Total points}} \text{Rng}(n) \times 0.25 \times \frac{\pi}{180} \times 0.5} \times 100\%, \quad (18)$$

where Rng(n) is a range to the nth estimate or zero if $SNR_h \leq 2$ dB (so the quantity in the denominator is the area covered by significant returns). The statistic in terms of coverage (e.g., invalid area) accounts for the fact that data points located farther away from the radar cover larger area than the ones which are closer due to beam broadening (this effect may be regarded as "range-dependent coverage"). The described effect can be observed in the last three columns of Table 1 (which provide percentages of invalid points and invalid area). In all cases, percentages for invalid points are smaller than percentages for invalid area. This shows that the actual percentage of an area covered by invalid correlation coefficient estimates is larger than the percentage which quantifies the contribution of these points to the total number of significant returns (on the average, percentages of invalid area are almost twice larger than those of invalid points, as given in the last row of Table 1). This is logical because the majority of invalid estimates are in the areas of low-to-moderate SNR (seen in Fig. 8 and indicated by simulations) typically located far from the radar (due to attenuation of electromagnetic waves on propagation). Consequently, invalid estimates at far away ranges produce larger area of "pink fringe" (i.e., the area of missing information) than would ensue if most of invalid estimates were located closer to the radar. This indicates that the invalid area statistic provides

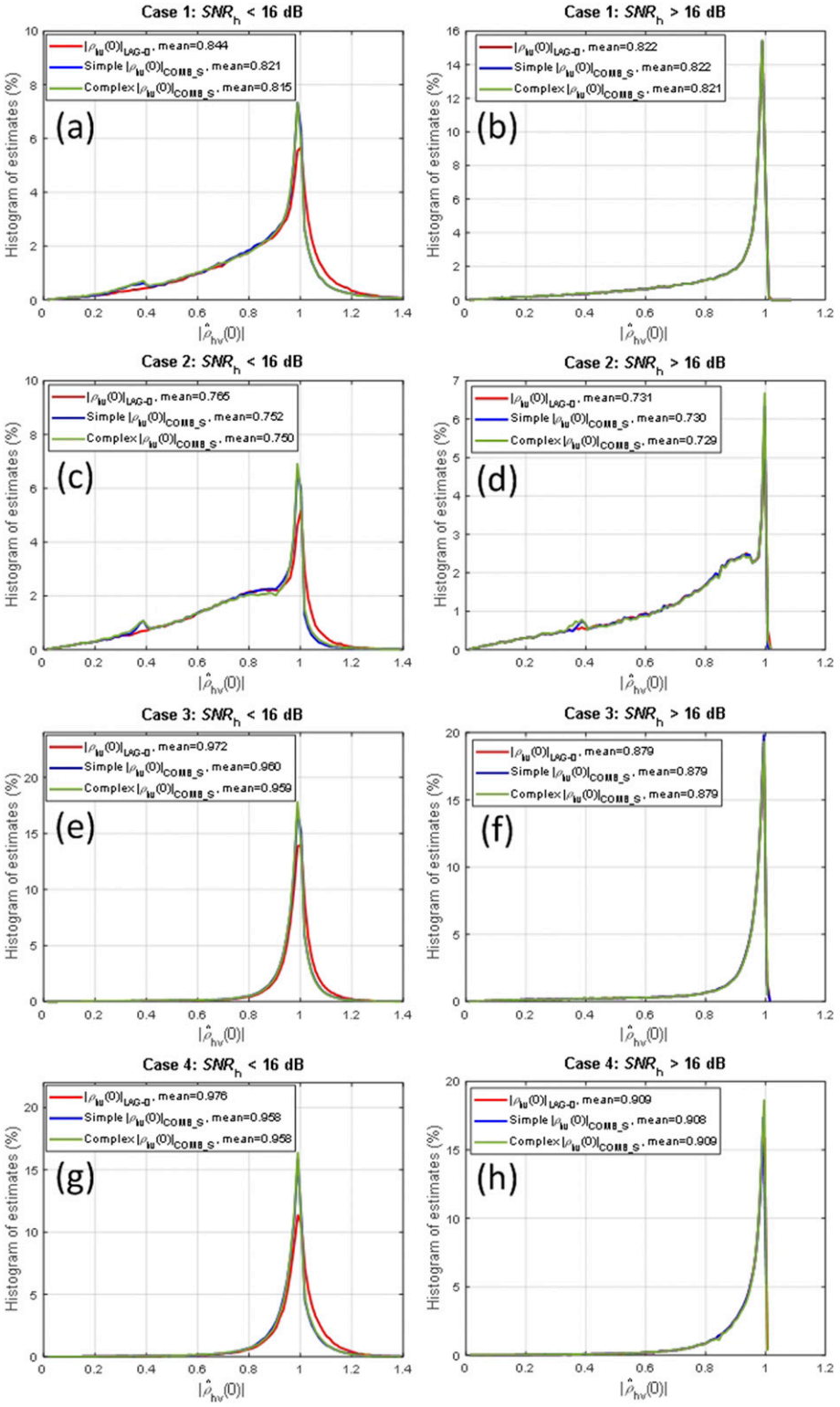

FIG. 9. Histogram of estimates in case of (left) $SNR_h < 16$ dB and (right) $SNR_h \geq 16$ dB for cases (a),(b) 1, (c),(d) 2, (e),(f) 3, and (g),(h) 4.

TABLE 1. Statistics showing the percentages of invalid estimates (invalid points; top value for each case) and area covered by them (invalid area; bottom value for each case) with respect to the total number of significant returns and area covered by them. A reduction in the number and the area covered by invalid estimates (with respect to invalid points and invalid area produced by the conventional estimator) is given in parentheses. All values are in percent.

		Simple	Complex
	$\lvert\hat{\rho}_{hv}(0)\rvert_{LAG\text{-}0}$	$\lvert\hat{\rho}_{hv}(0)\rvert_{COMB\_S}$	$\lvert\hat{\rho}_{hv}(0)\rvert_{COMB\_S}$
Case 1	16.7	11.04 (−33.82)	10.8 (−35.03)
	32.14	20.44 (−36.41)	19.87 (−38.2)
Case 2	10.02	5.06 (−49.54)	5.42 (−45.93)
	23.83	11.3 (−52.62)	11.83 (−50.36)
Case 3	25.41	16.88 (−33.59)	16.12 (−36.58)
	42.28	29.56 (−30.09)	28.04 (−33.68)
Case 4	21.18	13.17 (−37.79)	13.05 (−38.36)
	38.89	25.87 (−33.48)	25.16 (−35.31)
Avg	18.325	11.54 (−38.685)	11.35 (−38.975)
	34.285	21.8 (−38.15)	21.26 (−39.3875)

accurate evaluation of the area percentage for which radar fails to provide correlation coefficient coverage with meaningful information. At the same time, the additional valid estimates yielded by $\lvert\hat{\rho}_{hv}(0)\rvert_{COMB\_S}$ which are located far away from the radar cover larger area (than the ones closer in) and produce larger reduction in invalid area than in invalid points. Hence, the reduction in invalid area is more likely to be larger than in invalid points for events that spread over larger area in range (e.g., widespread stratiform precipitation) while the two statistics are more likely to produce similar results for an event that covers smaller area (e.g., an isolated convective supercell situation). Further, information in the second column of Table 1 may be found useful as it measures the portion of significant returns (e.g., returns for which $SNR_h > 2$ dB) associated with invalid correlation coefficient estimates as well as the percentage of area (covered by significant returns) for which valid information about correlation coefficient is missing when the conventional estimator is used . Thus, if for a given case, these percentages are rather small, it is unlikely that the $\lvert\hat{\rho}_{hv}(0)\rvert_{COMB\_S}$ application would result in significant improvement and vice versa. In all presented cases the invalid points (invalid area) percentages are 10% (20%) or more if $\lvert\hat{\rho}_{hv}(0)\rvert_{LAG\text{-}0}$ is used (second column of Table 1). On the average, the simple $\lvert\hat{\rho}_{hv}(0)\rvert_{COMB\_S}$ reduces invalid point (invalid area) percentages by 6.785% (12.585%) from 18.325% (34.385%) to 11.54% (21.8%). As expected, the improvement in invalid area is larger than in invalid points.

The last column in Table 1 illustrates that the complex $\lvert\hat{\rho}_{hv}(0)\rvert_{COMB\_S}$ produces slightly less invalid estimates (as well as area covered by them) than the simple $\lvert\hat{\rho}_{hv}(0)\rvert_{COMB\_S}$ in all cases except in case 2 and on the average 0.19% less invalid points as well as 0.54% smaller invalid area. The small differences in the number of valid estimates are likely due to the disparities in performance as indicated by simulations in Figs. 3d–f. In that regard, the reason that the simple $\lvert\hat{\rho}_{hv}(0)\rvert_{COMB\_S}$ produces slightly less number of invalid estimates than the complex $\lvert\hat{\rho}_{hv}(0)\rvert_{COMB\_S}$ in case 2 is most likely because the returns with spectrum widths around 1 m s^{-1} dominate in the areas where majority of additional valid estimates are produced (in which case the simple $\lvert\hat{\rho}_{hv}(0)\rvert_{COMB\_S}$ yields marginally more valid estimates than the complex $\lvert\hat{\rho}_{hv}(0)\rvert_{COMB\_S}$, as indicated by simulations in Fig. 3d). However, the reason that the complex $\lvert\hat{\rho}_{hv}(0)\rvert_{COMB\_S}$ performs slightly better in the majority of cases is likely because most additional valid estimates are at larger distances where resolution volumes [i.e., volumes encompassed by the radar beam illuminating scatterers of interest and denoted as V_6 in Doviak and Zrnić (1993)] are larger and contain more scatterers which tend to produce higher spectrum widths. If so, this corroborates simulation results presented in Fig. 3f which infer that the complex $\lvert\hat{\rho}_{hv}(0)\rvert_{COMB\_S}$ produces slightly more valid estimates than the simple $\lvert\hat{\rho}_{hv}(0)\rvert_{COMB\_S}$ at σ_v of ~4 m s^{-1}.

The numbers within parentheses in the last two columns of Table 1 also illustrate the percentage reduction in invalid points (invalid points reduction) and invalid area (invalid area reduction) yielded by the simple and complex $\lvert\hat{\rho}_{hv}(0)\rvert_{COMB\_S}$ and in relation to the same quantities produced by the conventional estimator. For the invalid points reduction, these are computed as

$$X \text{ invalid points reduction} = \left[\frac{\sum_{n=1}^{\text{Total points}} X^{\text{INV}}(n)}{\sum_{n=1}^{\text{Total points}} \lvert\hat{\rho}_{hv}(0)\rvert^{\text{INV}}_{\text{LAG-0}}(n)} - 1\right] \times 100\%. \quad (19)$$

The invalid area reduction is computed as

$$X \text{ invalid area reduction} = \left[\frac{\sum_{n=1}^{\text{Total points}} X^{\text{INV}}(n) \times \text{Rng}(n) \times 0.25 \times \frac{\pi}{180} \times 0.5}{\sum_{n=1}^{\text{Total points}} \lvert\hat{\rho}_{hv}(0)\rvert^{\text{INV}}_{\text{LAG-0}}(n) \times \text{Rng}(n) \times 0.25 \times \frac{\pi}{180} \times 0.5} - 1\right] \times 100\%. \quad (20)$$

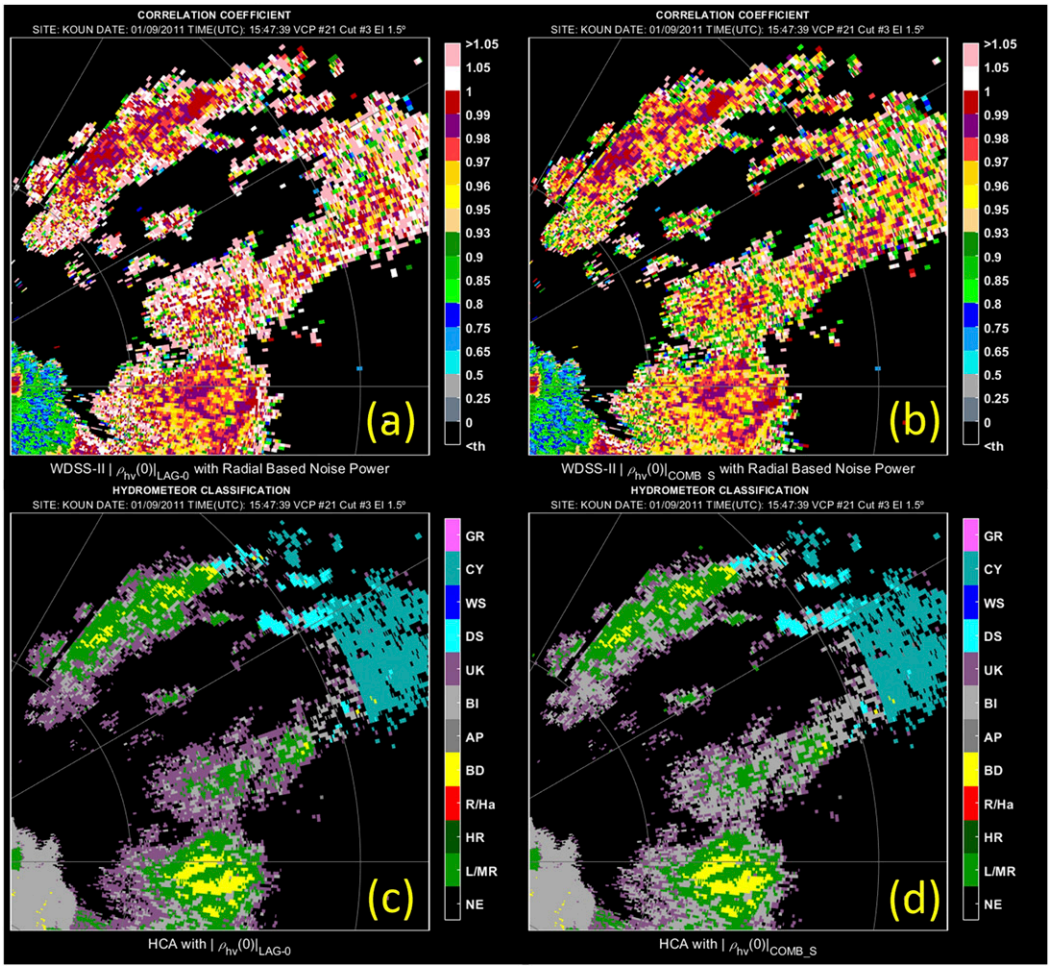

FIG. 10. (top) Smoothed correlation coefficient fields generated using WDSS-II from (a) $|\hat{\rho}_{hv}(0)|_{LAG\text{-}0}$ and (b) simple $|\hat{\rho}_{hv}(0)|_{COMB\_S}$ estimators. (bottom) HCA fields generated using WDSS-II with (c) $|\hat{\rho}_{hv}(0)|_{LAG\text{-}0}$, and (d) simple $|\hat{\rho}_{hv}(0)|_{COMB\_S}$ estimators.

In terms of invalid points, the average reduction delivered by the simple $|\hat{\rho}_{hv}(0)|_{COMB\_S}$ is 38.685% and 38.975% by the complex $|\hat{\rho}_{hv}(0)|_{COMB\_S}$. In case of invalid area reduction, these percentages are 38.15% and 39.3875%. Note that because only invalid estimates are considered, the invalid points reduction and invalid area reduction statistics are comparable (i.e., since most invalid estimates are concentrated farther away from the radar, the range-dependent coverage effect is small). As in the previous comparisons, the differences between the performances of the simple and complex $|\hat{\rho}_{hv}(0)|_{COMB\_S}$ are small.

So far, an extensive analysis of the proposed estimation technique performance via histograms (Fig. 9) and statistics (Fig. 8, Table 1, and appendix B) has been given. It demonstrates that $|\hat{\rho}_{hv}(0)|_{COMB\_S}$ produces quantifiable decrease in the number of invalid estimates as well as the area covered by these estimates which ultimately results in the decreased amount of missing information in the correlation coefficient fields. Furthermore, the histogram means (Fig. 9) corroborate simulation results and infer that both the simple and complex $|\hat{\rho}_{hv}(0)|_{COMB\_S}$ produce more accurate (i.e., less biased) estimates than $|\hat{\rho}_{hv}(0)|_{LAG\text{-}0}$ in the areas of low-to-moderate SNR. Nonetheless, the question arises whether these improvements would help forecasters in the field (e.g., radar meteorologists assessing the situation and making predictions based on the fields of radar products) and/or whether these may result in improved outputs of weather radar algorithms. Gauging former is beyond the scope of this paper but to compare the effects of simple $|\hat{\rho}_{hv}(0)|_{COMB\_S}$ and $|\hat{\rho}_{hv}(0)|_{LAG\text{-}0}$ application on HCA outputs, the estimates of spectral moments and polarimetric variables from case 4 were ingested into the WDSS-II software (Lakshmanan et al. 2007) which produced the HCA fields in Fig. 10. Note that the

fields in Fig. 10 are a subsection of the entire field encompassed by the yellow rectangle in Fig. 7f. The spatially smoothed estimates of $|\rho_{hv}(0)|$ (Lakshmanan 2004) produced by the WDSS-II software using $|\hat{\rho}_{hv}(0)|_{LAG\text{-}0}$ and simple $|\hat{\rho}_{hv}(0)|_{COMB\_S}$ are shown in Figs. 10a and 10b, respectively. The corresponding HCA outputs (Figs. 10c,d) reveal a decreased number of points classified as ''unknown'' (labeled UK in Figs. 10c,d) in the HCA field obtained from the simple $|\hat{\rho}_{hv}(0)|_{COMB\_S}$ estimates. Overall, the total number of points classified as ''unknown'' decreased from 21 958 (covering 2682.27 km^2) to 17 132 (covering 1956 km^2), which is ~22% (~27.1%) reduction.

5. Summary and conclusions

Herein, a simple hybrid technique designed to produce copolar correlation coefficient estimates at low-to-moderate SNRs (i.e., for SNRs less than 20 dB) for unambiguous velocities on the order of $v_a = \sim 9\,m\,s^{-1}$ (e.g., surveillance scans of the WSR-88) is presented. The technique addresses the issue present in the conventional lag-0 estimator (currently in use on the WSR-88D network) where the positive bias of the estimator increases exponentially with SNR reduction. The positive bias results in the visibly increased number of invalid correlation coefficient estimates (values exceeding 1.0) in areas of SNR lower than ~15 dB. Application of the technique to simulated time series shows that the proposed technique yields $|\rho_{hv}(0)|$ estimates with smaller biases compared to the conventional lag-0 estimator at low-to-moderate SNRs. At the same time, a standard deviation of estimates is comparable to that of the lag-0 estimator at all SNRs. Results obtained using simulated time series also indicate that the application of the technique will result in a decreased number of invalid estimates. Further, the algorithms which rely on the $|\rho_{hv}(0)|$ measurements may benefit from the less biased estimates and yield outputs with improved accuracy.

Four examples, produced using actual WSR-88D data, are used to demonstrate the improvement in the quality of $|\rho_{hv}(0)|$ fields resulting from the application of the technique. Visual inspection of the results obtained using the proposed technique revealed visible improvement in the number of valid estimates with respect to the conventional lag-0 estimator. As predicted by simulations, the most visible decrease in the frequency of invalid estimates is in the areas of weak radar returns. This is further corroborated by the plots which present the percentage of valid estimates as a function of SNR as well as the histograms of estimates where the differences between the improved and conventional estimates are visible at low-to-moderate SNRs but do not exhibit significant differences at higher SNRs. The improvements are also quantified in terms of percentages of invalid estimates as well as the area covered by such estimates. For the four presented examples, the conventional estimator produced 18.325% of invalid estimates (with respect to the total number of significant returns) which covered 34.285% of the total area covered by significant returns. The proposed estimation technique reduced the average number of invalid estimates and the corresponding area by 6.785% and 12.585%, respectively. The latter percentage is almost 2 times larger than the former because the majority of valid estimates, gained by the use of the proposed technique, are typically located farther away from the radar and therefore cover larger area than significant returns that are closer in. This produces the effect whereby the reduction in total area covered by invalid estimates is typically larger than the reduction in the number of such estimates for weather events which spread over large area in range. If the reduction is expressed using the reference quantities produced by the conventional estimator (in which case the focus in only on the areas where most invalid estimates are located), the use of an estimation technique proposed here results in an average of ~39% reduction (based on four examples shown) in both the number of invalid estimates as well as the area covered by them.

The proposed technique was also tested for the effects on the HCA outputs. In the presented example, the HCA field obtained using the improved estimator exhibited a reduction of ~22% in the number of classifications labeled as ''unknown'' compared to the same field produced using the conventional estimator. If expressed in terms of the area covered by the ''unknown'' classifications, the reduction was ~27.1%. This was the result of the increased number of valid estimates and the improved accuracy of estimates produced by the estimation technique described herein.

The results presented in this work demonstrate considerable improvement in the fields of correlation coefficient estimates yielded by the proposed estimation technique. Nonetheless, both visual examinations and the presented statistic indicate that a significant number of invalid estimates persist despite the improvements. In that regard, correlation coefficient quality could be further enhanced by exploring techniques to reduce the standard deviation of estimates since the proposed estimation technique presented here improves upon bias but not standard deviation. Note that the correlation coefficient estimates are more sensitive to standard deviation impacts than other polarimetric variables at

low-to-moderate SNRs. Thus, a weighted range average in these areas is one possible technique to reduce the variability of correlation coefficient estimates as demonstrated in Ivić and Isom (2014).

The estimation technique for improving correlation coefficient estimates presented here is much simpler than the complex technique proposed in Ivić (2016). Compared to the latter technique, biases of estimates are improved adequately with the simple technique while retaining the benefits of increased number of valid estimates as well as the reduced bias over the conventional estimator.

Acknowledgments. The author would like to thank Dr. Sebastián Torres and Dr. Chris Curtis as well as anonymous reviewers for providing comments that improved this manuscript. Funding was provided by NOAA/Office of Oceanic and Atmospheric Research under NOAA–University of Oklahoma Cooperative Agreement NA11OAR4320072, U.S. Department of Commerce. The statements, findings, conclusions, and recommendations are those of the author(s) and do not necessarily reflect the views of NOAA or the U.S. Department of Commerce.

APPENDIX A

Algorithm Description

In this appendix, an algorithm is described whereby $|\hat{\rho}_{hv}(0)|_{LAG\text{-}0}$, $|\hat{\rho}_{hv}(0)|_{LE\_1}$, and $|\hat{\rho}_{hv}(0)|_{LE\_2}$ are combined to produce less biased estimates of $|\rho_{hv}(0)|$ denoted as $|\hat{\rho}_{hv}(0)|_{COMB\_S}$. It is as follows:

If $|\hat{\rho}_{hv}(0)|_{LAG\text{-}0} \le 0.4$ or $SNR_h \le -2$ dB or $SNR_v \le -2$ dB then $|\hat{\rho}_{hv}(0)|_{COMB\_S} = |\hat{\rho}_{hv}(0)|_{LAG\text{-}0}$ and exit.

else compute

$$\text{temp\_val} = \left[|\hat{\rho}_{hv}(0)|_{LAG-0} + |\hat{\rho}_{hv}(0)|_{LE\_1}\right]/2$$

If [temp_val ≤ 1 or (temp_val > 1 and $|\hat{\rho}_{hv}(0)|_{LAG\text{-}0} > 1$ and temp_val $< |\hat{\rho}_{hv}(0)|_{LAG\text{-}0}$)] and [$|\hat{\rho}(1)|_{hv} > 0.8$ or $SNR_h < 12$ dB] then

$$|\hat{\rho}_{hv}(0)|_{COMB\_S} = temp\_val$$

else

$$|\hat{\rho}_{hv}(0)|_{COMB\_S} = |\hat{\rho}_{hv}(0)|_{LAG\text{-}0}.$$

If [$|\hat{\rho}_{hv}(0)|_{LE\_1} \le 1$ and $|\hat{\rho}_{hv}(0)|_{COMB\_S} > 1$] or [$|\hat{\rho}_{hv}(0)|_{LE\_1} > 1$ and $|\hat{\rho}_{hv}(0)|_{COMB\_S} > 1$ and $|\hat{\rho}_{hv}(0)|_{LE\_1} < |\hat{\rho}_{hv}(0)|_{COMB\_S}$] then

$$|\hat{\rho}_{hv}(0)|_{COMB\_S} = |\hat{\rho}_{hv}(0)|_{LE\_1}.$$

If $SNR_h > 0$ dB and $SNR_v > 0$ dB and [$|\hat{\rho}(1)|_{hv} > 0.85$ or ($|\hat{\rho}(1)|_{hv} > 0.6$ and $SNR_h > 10$ dB)] and [($|\hat{\rho}_{hv}(0)|_{LE\_2} \le 1$ and $|\hat{\rho}_{hv}(0)|_{COMB\_S} > 1$) or ($|\hat{\rho}_{hv}(0)|_{LE\_2} > 1$ and $|\hat{\rho}_{hv}(0)|_{COMB\_S} > 1$ and $|\hat{\rho}_{hv}(0)|_{LE\_2} < |\hat{\rho}_{hv}(0)|_{COMB\_S}$)] then

$$|\hat{\rho}_{hv}(0)|_{COMB\_S} = |\hat{\rho}_{hv}(0)|_{LE\_2},$$

where

$$|\hat{\rho}(1)|_{hv} = \frac{|\hat{R}_h(1)|}{2\hat{S}_h} + \frac{|\hat{R}_v(1)|}{2\hat{S}_v}. \tag{A1}$$

In the first step of the algorithm $|\hat{\rho}_{hv}(0)|_{COMB\_S}$ is set to $|\hat{\rho}_{hv}(0)|_{LAG\text{-}0}$ unless $|\hat{\rho}_{hv}(0)|_{LAG\text{-}0} > 0.4$, $SNR_h > -2$ dB and $SNR_v > -2$ dB. This is done because it was found that the value of $|\hat{\rho}_{hv}(0)|_{LAG\text{-}0}$ hardly ever takes values below 0.4 if $|\rho_{hv}(0)| \ge 0.8$ (due to statistical fluctuations), which suggests that an estimate improvement is not needed if $|\hat{\rho}_{hv}(0)|_{LAG\text{-}0} \le 0.4$ (since the technique is designed to improve the estimates of $|\rho_{hv}(0)|$ that are of most interest and are therefore above 0.8). Further, it was found that the computations of $|\hat{\rho}_{hv}(0)|_{LE\_1}$ and $|\hat{\rho}_{hv}(0)|_{LE\_2}$ are unreliable due to the increasingly large standard deviations of estimates if SNR_h or SNR_v are less than -2 dB. Because of this, $|\hat{\rho}_{hv}(0)|_{COMB\_S}$ is set to $|\hat{\rho}_{hv}(0)|_{LAG\text{-}0}$ if SNR_h or SNR_v are less than -2 dB. In the second step, $|\hat{\rho}_{hv}(0)|_{LAG\text{-}0}$ and $|\hat{\rho}_{hv}(0)|_{LE\_1}$ are averaged to equalize the biases since the first estimator exhibits increasingly positive and the second increasingly negative bias as $|\rho(m)|$ decreases. The next step is to use this average only if it yields a valid value (i.e., between 0 and 1) or is closer to one than the currently available estimate pending the conditions that $|\hat{\rho}(1)|_{hv} > 0.8$ or $SNR_h < 12$ dB. Next, to increase the number of valid estimates, $|\hat{\rho}_{hv}(0)|_{COMB\_S}$ is set to $|\hat{\rho}_{hv}(0)|_{LE\_1}$ if the first is invalid but the latter is not or if both are invalid but $|\hat{\rho}_{hv}(0)|_{LE\_1}$ is closer to one. The final step utilizes $|\hat{\rho}_{hv}(0)|_{LE\_2}$ to further increase the number of valid estimates pending the set of conditions designed to optimize the bias performance.

APPENDIX B

Statistic Based on Valid Estimates

In this appendix, Table B1 presents a comprehensive statistic for $SNR_h > 2$ dB (top section) and for $2 < SNR_h < 16$ dB (bottom section). It gives the number of valid estimates (i.e., valid points) for each of the three estimators as well as the total points (i.e., number of locations for which $SNR_h > 2$ dB and $2 < SNR_h < 16$ dB)

TABLE B1. Statistics for $SNR_h > 2$ dB and $2 < SNR_h < 16$ dB. For each case, the top value is points and the bottom value is area (km^2).

	M	v_a ($m\,s^{-1}$)	Total	$\lvert\hat{\rho}_{hv}(0)\rvert_{LAG\text{-}0}$	Simple $\lvert\hat{\rho}_{hv}(0)\rvert_{COMB\_S}$	Complex $\lvert\hat{\rho}_{hv}(0)\rvert_{COMB\_S}$
$SNR_h > 2$ dB						
Case 1	16	7.97	291 118	242 538 or 83.3%	258 966 or 88.96%	259 554 or 89.2%
			69 108.02	46 891.17 or 67.86%	54 979.84 or 79.56%	55 376.19 or 80.13%
Case 2	29	8.7	289 391	260 389 or 89.98%	274 756 or 94.94%	273 709 or 94.58%
			46 600.95	35 495.8 or 76.17%	41 339.21 or 88.7%	41 088.84 or 88.17%
Case 3	29	9	269 044	200 677 or 74.59%	223 640 or 83.12%	225 684 or 83.88%
			52 019.76	30 026.31 or 57.72%	36 643.36 or 70.44%	37 434.087 or 71.96%
Case 4	29	9	193 324	152 386 or 78.82%	167 858 or 86.83%	168 088 86.95%
			22 281.9	13 616.85 or 61.11%	16 517.81 or 74.13%	16 676.55 or 74.84%
$2 < SNR_h < 16$ dB						
Case 1	16	7.97	176 501 or 60.63%	129 564 or 73.4%	144 918 or 82.1%	145 578 or 82.5%
			50 001.3 or 72.35%	28 647.51 or 57.3%	36 174.09 or 72.34%	36 602.99 or 73.2%
Case 2	29	8.7	185 716 or 64.17%	158 026 or 85.1%	171 500 or 92.34%	170 634 or 91.88%
			38 894.06 or 83.46%	28 149.59 or 72.36%	33 743.78 or 86.76%	33 535.91 or 86.22%
Case 3	29	9	167 504 or 62.26%	100 378 or 59.93%	122 662 or 73.23%	124 715 or 74.45%
			45 240.36 or 86.97%	23 430.14 or 51.79%	29 931.32 or 66.16%	30 724.99 or 67.91%
Case 4	29	9	96 048 or 49.68%	56 028 or 58.33%	70 963 or 73.88%	71 253 or 74.18%
			17 154.22 or 76.99%	8612.33 or 50.21%	11 435.71 or 66.66%	11 598.92 or 67.62%

for the four cases. Also, a percentage of valid estimates produced by each estimator is given. It is computed as

$$X \text{ valid points} = \frac{X \text{ valid points}}{\text{total points}} \times 100\%, \tag{B1}$$

where X is $\lvert\hat{\rho}_{hv}(0)\rvert_{LAG\text{-}0}$, simple $\lvert\hat{\rho}_{hv}(0)\rvert_{COMB\_S}$, or complex $\lvert\hat{\rho}_{hv}(0)\rvert_{COMB\_S}$. Further, a statistic in terms of area covered by valid estimates (i.e., valid area) is given. For a particular estimator, it is computed as

$$X \text{ valid area}\,(\text{km}^2) = \sum_{n=1}^{\text{Total points}} X^{\text{VAL}}(n) \times \text{Rng}(n) \times 0.25 \times \frac{\pi}{180} \times 0.5, \tag{B2}$$

where $X^{\text{VAL}}(n)$ is one if nth estimate from an estimator X is valid and zero otherwise. Then, the percentage of area covered by valid estimates produced by an estimator X is

$$X \text{ valid area} = \frac{X \text{ valid area } (\text{km}^2)}{\sum_{n=1}^{\text{Total points}} \text{Rng}(n) \times 0.25 \times \frac{\pi}{180} \times 0.5} \times 100\%, \tag{B3}$$

where the value in the denominator of (B3) is the total area covered by significant returns (i.e., total area in kilometers for returns with $SNR_h > 2$ dB and $2 < SNR_h < 16$ dB in Table B1). The range-dependent coverage effect can be observed in the fourth column of the $2 < SNR_h < 16$ dB results in Table B1 (which provides total points and total area for data points with low-to-moderate SNR between 2 and 16 dB). In all cases, percentages for total points in this column are smaller than percentages for total area. This shows that the actual percentage of an area covered by data points with low-to-moderate SNR is larger than the percentage which quantifies the contribution of these points to the total number of significant returns. This further corroborates that the majority of data points with low-to-moderate SNR are located far from the radar (which is a result of propagation attenuation).

The results in Table B1 show that both the simple and complex $\lvert\hat{\rho}_{hv}(0)\rvert_{COMB\_S}$ produce consistently more valid estimates as well as larger valid area than $\lvert\hat{\rho}_{hv}(0)\rvert_{LAG\text{-}0}$. It is interesting to note that, for all cases, the percentage of valid estimates (i.e., valid points) is higher than the valid area percentage for each estimator in both sections of Table B1. This is because most invalid estimates are located farther away from the radar which results in valid area being typically smaller than the corresponding number of valid points due to the range-dependent coverage effect. Furthermore, the percentages in the last three columns in the top section of Table B1 are higher than in the corresponding columns in the bottom section of Table B1. This is expected as the probability of invalid estimates increases as SNR decreases resulting in lower percentage of valid estimates as well as valid area for $2 < SNR_h < 16$ dB than for $SNR_h > 2$ dB.

Comparison statistics are given in Table B2, where the differences among the last three columns of Table B1 are computed. Results in the top section of Table B2 show that the simple and complex $\lvert\hat{\rho}_{hv}(0)\rvert_{COMB\_S}$ yield

TABLE B2. Difference statistics for $SNR_h > 2$ dB and $2 < SNR_h < 16$ dB. For each case, the top value is the difference in the number of valid points and the bottom value is the difference in valid area (km^2).

	Simple $\lvert\hat{\rho}_{hv}(0)\rvert_{COMB\_S}$ vs $\lvert\hat{\rho}_{hv}(0)\rvert_{LAG\text{-}0}$	Complex $\lvert\hat{\rho}_{hv}(0)\rvert_{COMB\_S}$ vs $\lvert\hat{\rho}_{hv}(0)\rvert_{LAG\text{-}0}$	Complex $\lvert\hat{\rho}_{hv}(0)\rvert_{COMB\_S}$ vs Simple $\lvert\hat{\rho}_{hv}(0)\rvert_{COMB\_S}$
$SNR_h > 2$ dB			
Case 1	16 428 or 5.66%	17 016 or 5.9%	588 or 0.24%
	8088.67 or 11.7%	8485.02 or 12.27%	396.35 or 0.57%
Case 2	14 367 or 4.96%	13 320 or 4.56%	−1047 or −0.4%
	5843.41 or 12.53%	5593.04 or 12%	−250.37 or −0.53%
Case 3	22 963 or 8.53%	25 007 or 9.29%	2044 or 0.76%
	6617.05 or 12.72%	7407.78 or 14.24%	790.73 or 1.52%
Case 4	15 472 or 8.01%	15 702 or 8.13%	230 or 0.12%
	2900.96 or 13.02%	3059.7 or 13.73%	158.74 or 0.71%
Avg	6.79%	6.97%	0.18%
	12.49%	13.06%	0.57%
$2 < SNR_h < 16$ dB			
Case 1	15 354 or 8.7%	16 014 or 9.1%	660 or 0.4%
	7526.58 or 15.04%	7955.48 or 15.9%	428.9 or 0.86%
Case 2	13 474 or 7.24%	13 474 or 6.78%	−866 or −0.46%
	5594.19 or 14.4%	5386.32 or 13.86%	−207.87 or −0.54%
Case 3	22 284 or 13.3%	24 337 or 14.52%	2053 or 1.23%
	6501.18 or 14.37%	7294.85 or 16.12%	793.67 or 1.75%
Case 4	14 935 or 15.55%	15 225 or 15.85%	290 or 0.3%
	2823.38 or 16.45%	2986.59 or 17.41%	163.21 or 0.96%
Avg	11.2%	11.85%	0.37%
	15.07%	15.82%	0.76%

on the average 6.79% and 6.97% more valid points as well as 12.49% and 13.06% larger valid area than $\lvert\hat{\rho}_{hv}(0)\rvert_{LAG\text{-}0}$, respectively. Hence, while the percentages of valid points are higher than valid area in the top section of Table B1, the improvement, yielded by the simple and complex $\lvert\hat{\rho}_{hv}(0)\rvert_{COMB\_S}$, is larger if expressed in valid area than in valid points. This is because the increase in valid estimates is prevalent in areas with low-to-moderate SNR (as shown by simulations and also in Figs. 8 and 9) which are typically situated farther away from the radar (therefore covering larger area as already stated). If only locations where $2 < SNR_h < 16$ dB are considered, the simple and complex $\lvert\hat{\rho}_{hv}(0)\rvert_{COMB\_S}$ yield on the average 11.2% and 11.85% more valid points as well as 15.07% and 15.82% larger valid area than $\lvert\hat{\rho}_{hv}(0)\rvert_{LAG\text{-}0}$, respectively (as shown in the bottom section of Table B2). Thus, as expected the improvement in low-to-moderate SNR areas is larger than the overall improvement presented in the top section of Table B2. The approximate difference in $\lvert\hat{\rho}_{hv}(0)\rvert_{COMB\_S}$ yielded improvements at the full SNR range (i.e., $SNR_h > 2$ dB) versus low-to-moderate SNR range (i.e., $2 < SNR_h < 16$ dB) is ~4% for the difference in valid points (i.e., approximate difference between the last rows of the second and third columns of Table B2) but 2.5% for the difference in valid area. The latter percentage is smaller because the data points with low-to-moderate SNRs contribute more to the total valid estimate coverage (due to their typical range location) than those with high SNR (that are usually closer to the radar). This effectively means that the points which belong to $2 < SNR_h < 16$ dB are typically weighed more than those that belong to $SNR_h \geq 16$ dB when computing the valid area (for weather events spread over large space). Hence, this reduces the difference between improvements in valid area at full and low-to-moderate SNRs compared to the same difference expressed in valid points. In the latter case, all data points are weighted the same and focusing only on those at low-to-moderate SNRs shows larger improvement; thus, further corroborating the conclusion that the proposed estimation technique yields most improvements in the weak signal areas.

REFERENCES

Andrić, J., M. R. Kumjian, D. S. Zrnić, J. M. Straka, and V. M. Melnikov, 2013: Polarimetric signatures above the melting layer in winter storms: An observational and modeling study. *J. Appl. Meteor. Climatol.*, **52**, 682–700, https://doi.org/10.1175/JAMC-D-12-028.1.

Balakrishnan, N., and D. S. Zrnić, 1990: Use of polarization to characterize precipitation and discriminate large hail. *J. Atmos. Sci.*, **47**, 1525–1540, https://doi.org/10.1175/1520-0469(1990)047<1525:UOPTCP>2.0.CO;2.

Brandes, E. A., and K. Ikeda, 2004: Freezing-level estimation with polarimetric radar. *J. Appl. Meteor.*, **43**, 1541–1553, https://doi.org/10.1175/JAM2155.1.

Brown, R. A., V. T. Wood, and D. Sirmans, 2002: Improved tornado detection using simulated and actual WSR-88D data with enhanced resolution. *J. Atmos. Oceanic Technol.*, **19**, 1759–1771, https://doi.org/10.1175/1520-0426(2002)019<1759:ITDUSA>2.0.CO;2.

Caylor, J., and A. J. Illingworth, 1989: Identification of the bright band and hydrometeors using co-polar dual polarization radar. Preprints, *24th Conf. on Radar Meteorology*, Tallahassee, FL, Amer. Meteor. Soc., 352–357.

Doviak, R. J., and D. S. Zrnić, 1993: *Doppler Radar and Weather Observations*. Academic Press, 562 pp.

——, V. Bringi, A. Ryzhkov, A. Zahrai, and D. Zrnić, 2000: Considerations for polarimetric upgrades to operational WSR-88D radars. *J. Atmos. Oceanic Technol.*, **17**, 257–278, https://doi.org/10.1175/1520-0426(2000)017<0257:CFPUTO>2.0.CO;2.

Friedrich, K., U. Germann, and P. Tabary, 2009: Influence of ground clutter contamination on polarimetric radar parameters. *J. Atmos. Oceanic Technol.*, **26**, 251–269, https://doi.org/10.1175/2008JTECHA1092.1.

Galati, G., and G. Pavan, 1995: Computer simulation of weather radar signals. *Simul. Pract. Theory*, **3**, 17–44, https://doi.org/10.1016/0928-4869(95)00009-I.

Giangrande, S. E., J. M. Krause, and A. V. Ryzhkov, 2008: Automatic designation of the melting layer with a polarimetric prototype of the WSR-88D radar. *J. Appl. Meteor. Climatol.*, **47**, 1354–1364, https://doi.org/10.1175/2007JAMC1634.1.

Harris, F. J., 1978: On the use of windows for harmonic analysis with the discrete Fourier transform. *Proc. IEEE*, **66**, 51–83, https://doi.org/10.1109/PROC.1978.10837.

Istok, M. J., and R. L. Ice, 2016: NEXRAD product improvement: Update 2016. *32nd Conf. on Environmental Information Processing Technologies*, New Orleans, LA, Amer. Meteor. Soc., 10.1, https://ams.confex.com/ams/96Annual/webprogram/Paper289554.html.

Ivić, I. R., 2014: On the use of a radial-based noise power estimation technique to improve estimates of the correlation coefficient on dual-polarization weather radars. *J. Atmos. Oceanic Technol.*, **31**, 1867–1880, https://doi.org/10.1175/JTECH-D-14-00052.1.

——, 2016: A technique to improve copolar correlation coefficient estimation. *IEEE Trans. Geosci. Remote Sens.*, **54**, 5776–5800, https://doi.org/10.1109/TGRS.2016.2572185.

——, and B. Isom, 2014: Methods to improve fields of correlation coefficient estimates. *Eighth European Conf. on Radar in Meteorology and Hydrology (ERAD)*, Garmisch-Partenkirchen, Germany, 071, http://www.pa.op.dlr.de/erad2014/programme/ShortAbstracts/071_short.pdf.

——, C. Curtis, and S. M. Torres, 2013: Radial-based noise power estimation for weather radars. *J. Atmos. Oceanic Technol.*, **30**, 2737–2753, https://doi.org/10.1175/JTECH-D-13-00008.1.

Lakshmanan, V., 2004: A separable filter for directional smoothing. *IEEE Geosci. Remote Sens. Lett.*, **1**, 192–195, https://doi.org/10.1109/LGRS.2004.828178.

——, T. Smith, G. J. Stumpf, and K. Hondl, 2007: The warning decision support system–integrated information. *Wea. Forecasting*, **22**, 596–612, https://doi.org/10.1175/WAF1009.1.

Liu, L., V. N. Bringi, V. Chandrasekar, E. A. Mueller, and A. Mudukutore, 1994: Analysis of the copolar correlation coefficient between horizontal and vertical polarizations. *J. Atmos. Oceanic Technol.*, **11**, 950–963, https://doi.org/10.1175/1520-0426(1994)011<0950:AOTCCC>2.0.CO;2.

Melnikov, V. M., and D. S. Zrnić, 2004: Simultaneous transmission mode for the polarimetric WSR-88D: Statistical biases and standard deviations of polarimetric variables. NOAA/NSSL Rep., 84 pp., https://www.nssl.noaa.gov/publications/wsr88d_reports/SHV_statistics.pdf.

——, and ——, 2007: Autocorrelation and cross-correlation estimators of polarimetric variables. *J. Atmos. Oceanic Technol.*, **24**, 1337–1350, https://doi.org/10.1175/JTECH2054.1.

NOAA, 2017: Operational modes and volume coverage patterns. WSR-88D meteorological observations: Part C: WSR-88D products and algorithms, Federal Meteorological Handbook 11, FCM-H11C-2017, Office of the Federal Coordinator for Meteorological Services and Supporting Research, 5-1–5-24, https://www.ofcm.gov/publications/fmh/FMH11/fmh11partC.pdf.

Tang, L., J. Zhang, C. Langston, J. Krause, K. Howard, and V. Lakshmanan, 2014: A physically based precipitation-nonprecipitation radar echo classifier using polarimetric and environmental data in a real-time national system. *Wea. Forecasting*, **29**, 1106–1119, https://doi.org/10.1175/WAF-D-13-00072.1.

Torres, S. M., and C. Curtis, 2007: Initial implementation of super-resolution data on the NEXRAD network. *23rd Conf. on IIPS,* San Antonio, TX, Amer. Meteor. Soc., 5B.10, https://ams.confex.com/ams/87ANNUAL/techprogram/paper_116240.htm.

——, and D. A. Warde, 2014: Ground clutter mitigation for weather radars using the autocorrelation spectral density. *J. Atmos. Oceanic Technol.*, **31**, 2049–2066, https://doi.org/10.1175/JTECH-D-13-00117.1.

Warde, D. A., 2015: Mitigating ground-clutter contamination on polarimetric Doppler weather radars. *37th Conf. on Radar Meteorology*, Norman, OK, Amer. Meteor. Soc., 7, https://ams.confex.com/ams/37RADAR/webprogram/Paper274708.html.

——, and S. M. Torres, 2015: Minimizing the impact of ground-clutter filtering along the zero-isodop in polarimetric Doppler weather radars. *31st Conf. on Environmental Information Processing Technologies*, Phoenix, AZ, Amer. Meteor. Soc., 11.5, https://ams.confex.com/ams/95Annual/webprogram/Paper267106.html.

Zrnić, D. S., 1975: Simulation of weatherlike Doppler spectra and signals. *J. Appl. Meteor.*, **14**, 619–620, https://doi.org/10.1175/1520-0450(1975)014<0619:SOWDSA>2.0.CO;2.

——, and R. J. Doviak, 1976: Effective antenna pattern of scanning radars. *IEEE Trans. Aerosp. Electron. Syst.*, **AES-12**, 551–555, https://doi.org/10.1109/TAES.1976.308254.